RSC Advances

REVIEW

View Article Online
View Journal | View Issue

Cite this: *RSC Adv.*, 2024, **14**, 23404

A review on carbon quantum dot/semiconductor-based nanocomposites as hydrogen production photocatalysts

Hareesh K *

Carbon quantum dots (CQDs) are discrete, quasi-spherical carbon nanoparticles with sizes below 10 nm. The properties of CQDs can be further enhanced by doping with elements such as nitrogen, phosphorous, sulphur, and boron or co-doping with heteroatoms such as nitrogen–phosphorous, nitrogen–sulphur, and nitrogen–boron. These excellent properties of CQDs can be utilized to enhance the photocatalytic performance of semiconductors. Therefore, in this review, we summarize different types of bare CQD-scaffolded semiconductors, both doped and co-doped, used for photocatalytic hydrogen production. Moreover, the detailed photocatalytic mechanism of CQD/semiconductor-based hydrogen production is reviewed. Recent progress in the design and development of CQD-based photocatalysts, along with the challenges involved, is comprehensively reviewed.

Received 6th June 2024
Accepted 10th July 2024

DOI: 10.1039/d4ra04149f

rsc.li/rsc-advances

1. Introduction

In 2004, Xu *et al.*[1] synthesized fluorescent carbon nanomaterials *via* electrophoresis and purification of arc discharge-produced single-walled carbon nanotubes. They also calculated the diameter of carbon nanomaterials to be 18.0 ± 0.4 nm through atomic force microscopy. Carbon dots (CDs) were first named carbon quantum dots by Sun *et al.* in 2006 when they synthesized nanoscale carbon particles with a quantum yield (QY) of only 10% using a carbon target and laser ablation method.[2] Because of the complicated preparation steps and low QY, no significant development was seen in this field till 2013. Nevertheless, in 2013, Yang's group developed CQDs with structures similar to polymers through a hydrothermal method using ethylenediamine and citric acid as precursors. As materials with the highest QY value, these CQDs achieved a QY up to 80%.[3] These CQDs can be used as functional nanocomposites and printing inks. The ease of usage, high QY, low toxicity, and strong photobleaching resistance of CQDs sparked a research boom and widespread interest.[4] Following this, researchers developed many approaches and technologies to pursue CQDs with high performance, and many important breakthroughs have occurred over the past few decades. Furthermore, CQDs differ from graphene quantum dots and carbonized polymer dots in terms of their distinct synthesis mechanisms, nanostructures, and features. Graphene quantum dots are anisotropic with lateral dimensions larger than their height,[5] whereas carbonized polymer dots exhibit spherical core–shell structures with a carbon core less than 20 nm.[6] Alternatively, CQDs are spherical in shape with a diameter less than 10 nm and are often produced from polymers or small molecules or biomass.

CQDs consist of few layers of graphite structures, and carbon atoms predominantly show sp^2 hybridization with surface groups. CQDs exhibit distinct properties such as solar light absorption, tunable fluorescence, up-conversion photoluminescence and unique electron accepting/donating behaviours.[6] Their fluorescence mechanism includes intrinsic state luminescence and the quantum confinement effect of size.[7] Fluorescence emissions from the visible to near-infrared range correspond to the radiative recombination of trapped photoinduced electrons and holes at different surface locations.[8] The optical absorption of CQDs correlates to the plasmon transition in the core of the dots. As CQDs are highly hydrophilic and amenable to functionalization

Department of Physics, Manipal Institute of Technology Bengaluru, Manipal Academy of Higher Education, Manipal 576104, India. E-mail: hareesh.k@manipal.edu

Hareesh K

Dr Hareesh K received his PhD (2014) from Mangalore University, India followed by Post-Doctoral Fellowship (2013–2017) from Savitribai Phule Pune University, India, and the University of Western Australia, Australia. Currently, he is an Assistant Professor–Senior Scale of Physics at the Department of Physics, Manipal Institute of Technology Bengaluru, Manipal Academy of Higher Education, Manipal, India. His research interests include the applications of 0D and 2D-based nanocomposites for energy storage and energy conversion.

with a wide range of chemical, polymeric, and biological species, they often have a variety of surface active functional groups such as amino, carbonyl, epoxy, hydroxyl, carboxylic acid and ether groups.[9] CQDs have attracted considerable attention owing to their less toxicity, good solubility, tunable fluorescence, superior electronic and catalytic properties,[8] which make them promising for applications in supercapacitors,[10] sensors,[11] solar cells,[12] light-emitting diodes[13–16] and photocatalytic hydrogen production.[17–19] However, the properties of CQDs can be amplified by creating new virtual energy levels originated by heteroatom dopants such as nitrogen,[20] phosphorus,[21] sulphur,[22] boron,[23] and selenium[24] and also by the co-doping atoms such as nitrogen–phosphorus,[25,26] nitrogen–sulphur,[27] and nitrogen–boron[28] leading to Fermi energy level shift close to the conduction band, boosting the faster exchange of electrons than pristine CQDs. Therefore, doped as well as co-doped CQDs have also gained interest in studying the photocatalytic activity for hydrogen production.[20–28] The summarized unique properties and synthesis techniques of CQDs are displayed in Fig. 1.

Considering the environmental issues such as depletion of fossil fuels and increased pollution, the other alternative renewable energy resources with the advantages of eco-friendliness, zero pollution and high energy storage capacity have attracted attention, and photocatalytic hydrogen production is one amongst them.[29] Photocatalytic hydrogen production involves water molecule splitting into oxygen and hydrogen using a catalyst in the presence of light, preferably in the visible region of sunlight.[30] The mechanism of water splitting into hydrogen using a photocatalyst can be summarized as follows. The water splitting, $2H_2O \rightarrow 2H_2 + O_2$, is a thermodynamically uphill reaction, which requires $\Delta G = 237$ kJ mol^{-1} (equivalent to an energy requirement of 1.23 eV). The corresponding photon energy is necessary both to store solar energy in the final products and to pass the activation energy barrier for the reaction, as shown in Fig. 2(A).[30]

The inset of Fig. 2(A) shows the schematic of a photocatalytic reaction in the presence of a photocatalyst. The electrons from the valence band were stimulated to the conduction band when the photocatalyst absorbs photons with energy equivalent to or higher than its band gap, leaving holes in the valence band (eqn (1)). Then, reduction half reaction (eqn (2)), *e.g.* for hydrogen evolution (eqn (3)), and oxidation half reaction (eqn (4)), for example, oxygen evolution for overall water splitting (eqn (5)), occur on the surface of the photocatalyst based on the type.[11]

$$\text{Photocatalyst} \xrightarrow{h\nu} e^- + h^+ \quad (1)$$

$$e^- + A \rightarrow A^- \quad (2)$$

where "A" is the electron acceptor.

$$2e^- + 2H^+ \rightarrow H_2 \quad (3)$$

$$h^+ + D \rightarrow D^+ \quad (4)$$

where "D" is the electron donor.

$$4h^+ + 2H_2O \rightarrow O_2 + 4H^+ \quad (5)$$

$$e^- + h^+ \rightarrow \text{light/heat} \quad (6)$$

Therefore, the minimum band gap for a suitable water splitting photocatalyst should be 1.23 eV. The band levels of various semiconductors are represented in Fig. 2(B).

The production of hydrogen from water using sunlight has advantages over other carbonaceous fossil fuels such as it is eco-friendly, it uses renewable energy sources, and it reduces

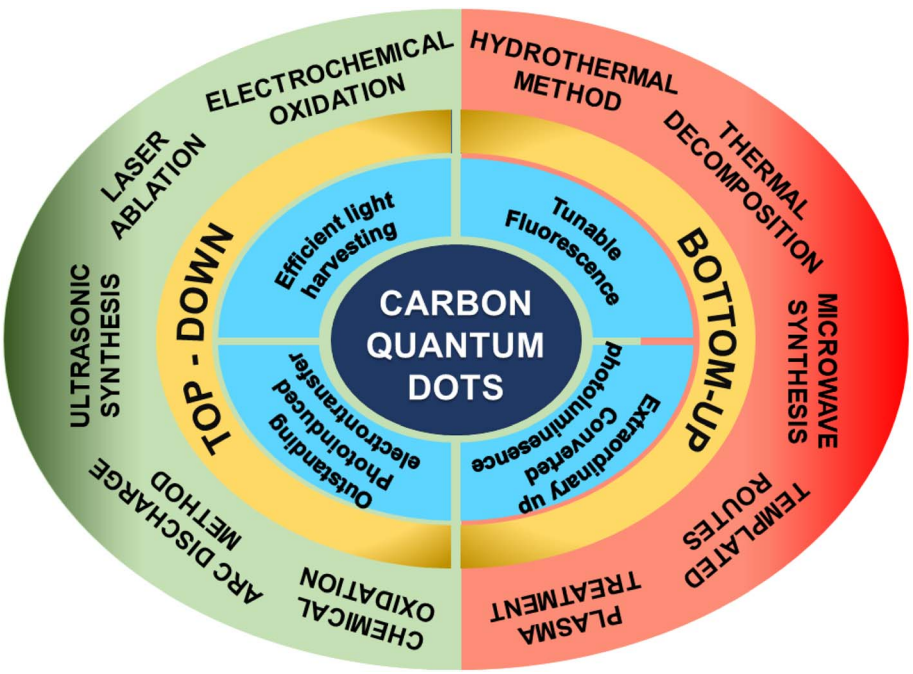

Fig. 1 CQDs with excellent properties and different synthesis techniques.

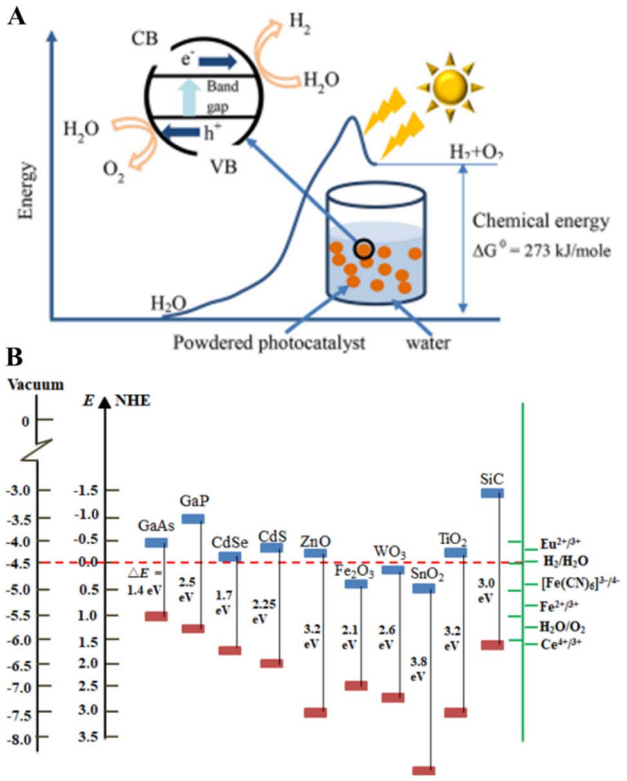

Fig. 2 (A) Schematic of the energy diagram of photocatalytic water splitting. (B) Energy band levels of different semiconductors. Inset in (A) shows the principle of photocatalytic water splitting. This figure has been reproduced from ref. 30 with permission from the Institute of Physics, Copyright 2021.

environmental pollution.[29,30] There are various catalysts available based on semiconductors for the photocatalytic production of hydrogen.[31–40] Nevertheless, the bandgap of most of the semiconductors (≥3.1 eV) lies in the ultraviolet region of electromagnetic spectrum. Therefore, it is needed to tune the band gap of semiconductors to the visible region (≤2.75 eV) by doping,[33] adding noble metals,[41] sensitizing with organic dye,[40] coupling with semiconductors,[42] and integrating with (i) 2D materials such as graphene,[43] MoS_2,[44] graphitic carbon nitride,[45] and WS_2,[46] (ii) 1D materials such as CNTs,[47] CdS nanowires,[48] and ZnO nanowires,[49] and (iii) 0D materials such as CQDs.[25,26]

Therefore, herein, we discuss the carbon quantum dot (doped and co-doped)/semiconductor-based nanocomposites for photocatalytic hydrogen production. Moreover, the different synthesis techniques for the development of CQD/semiconductor-based nanocomposites, and the challenges involved in enhancing the photocatalytic activity efficacy are discussed along with the summary.

2. Synthesis of CQD/semiconductor-based photocatalytic hydrogen production catalysts

CQDs can be synthesised by both top-down and bottom-up approaches. The summarized synthesis techniques of CQDs are shown in Fig. 1. The development of CQDs/semiconductors is a two-step synthesis method in most of the cases, and three steps in some cases. Yu *et al.* have synthesized CQDs by an alkali-assisted electrochemical method followed by the synthesis of CQD/TiO_2 nanocomposites by a hydrothermal method.[50] The CQDs and TiO_2 nanosheets were synthesized separately by electrochemical and hydrothermal methods respectively, followed by CQD/TiO_2 synthesis by thermal heating.[51] CQDs synthesized by a microwave-assisted method were employed to synthesize CQDs/TiO_2 by a hydrothermal method.[52] Zhang *et al.*[53] synthesized CQDs/TiO_2 by ultrasonication for 1 h followed by magnetic stirring. Zhou *et al.*[54] have synthesized CQD/Pt/TiO_2 nanocomposites by co-thermolysis of citric acid and TiO_2. The microwave-assisted method was employed to synthesize nitrogen, phosphorus co-doped CQDs followed by decoration of co-doped CQDs on TiO_2 nanoparticles by a hydrothermal method.[25] The CQDs were prepared by electrolysis of graphite rods followed by coupling with TiO_2 by a hydrothermal method.[55] Recently, Huang *et al.*[56] have synthesized CQDs by a hydrothermal method and decorated them on TiO_2 by a solvothermal method. Wang *et al.*[57] have synthesized CQDs by thermalizing citric acid and MoS_2/CQDs by a photoreduction process. They also prepared ternary MoS_2/CQD/$ZnIn_2S_4$ nanocomposites by a hydrothermal method. The nitrogen, phosphorus co-doped CQDs synthesized by the microwave-assisted method were decorated on ZnO nanorods by a hydrothermal method.[26] Qu *et al.* have prepared CQDs and $KNbO_3$ separately by a hydrothermal method and then prepared CQD/$KNbO_3$ nanocomposites by a simple stirring method under ambient conditions.[58] Wang *et al.*[59] have synthesized CQDs by a pyrolysis method, CdS by a solvothermal method, and then CQD/CdS by a simple stirring method for 12 h. Li *et al.*[60] have prepared CQDs and Ag–In–Zn–S (AIZS) quantum dots separately by electrochemical etching and hydrothermal methods respectively. Then, the composite of CQD/AIZS was developed hydrothermal treatment. All these procedures were followed by filtration/centrifugation of the product to remove unreacted precursors and washed with excess of double-distilled water and ethanol. Then, it was dried (under ambient conditions/vacuum) at 60–80 °C overnight. Overall, all these methods have their own advantages, for example, in terms of their use and control over reaction time and temperature, and the properties can be tuned, as well as disadvantages such as poor control over shape, crystallinity, and purification after synthesis technique. Nevertheless, green methods such as microwave and sonochemical are always on demand as they are eco-friendly.[61] Recently, Xu *et al.*[62] have adopted a hydrothermal method to prepare coal-based CQDs, nitrogen-doped CQDs and nitrogen, sulfur co-doped CQDs. The same research group has also used ultrasound-assisted hydrogen peroxide to covert coal to into high-value coal-based CQDs and sulfur-doped CQDs.[63] Many reports in the literature discuss the synthesis of CQDs and their characterizations. Nonetheless, the band gap tuning of the CQDs and CQD/semiconductor-based nanocomposites is sparse. The synthesis method can be used to control the size of the CQDs, tuning the band gap of semiconductors using CQDs and also to disperse the CQDs, which further enhance the efficiency of the photocatalytic activity of the developed CQDs/semiconductor. Yashwanth *et al.*[25] have co-

doped nitrogen–phosphorous into CQDs and then decorated them on TiO_2 nanoparticles. The weight percentage of CQDs was varied to tune the band gap of TiO_2 by a hydrothermal method, which enhanced the photocatalytic hydrogen production. The concentration of H_2O_2 was varied during the synthesis of CQDs to tune their band gap by Jia *et al.*[64] They argued that the band gap increased with the increase in the concentration of H_2O_2 and found to be less at 10% of H_2O_2, which suggests that the photocatalytic hydrogen can be tuned by varying the concentration of H_2O_2 during the synthesis of CQDs. Mehta *et al.*[65] have tuned the band gap of spherical CQDs, which were synthesized by a microwave radiation-assisted method, by fabricating Au@CQD core–shell composites. The band gap of CQDs was found to be 2.78 eV and it decreased to 2.68 eV for Au@CQD composites. The microwave radiation-assisted-synthesized nitrogen–phosphorous co-doped CQDs were also utilized to tune the band gap of ZnO, which, in turn, tuned its photocatalytic hydrogen production.[26] The carbonization process *via* a hydrothermal method was adopted to synthesize CQDs and then to construct the heterojunction of $BaZrO_{3-\delta}$ *via* a hydrothermal method.[66] Gogoi *et al.*[67] have synthesized CQDs by a hydrothermal method and CdS by a solvothermal method separately, and then used a simple chemical deposition method to prepare CQD/CdS composites. The ternary $LaFeO_3$/CdS/CQD nanocomposite was synthesized *via* a simple hydrothermal process by Manchala *et al.*[68] Hou *et al.*[69] have adopted a three-step synthesis procedure for the synthesis of CQD/γ-TaON heterojunctions. The individually synthesized CQDs (by alkali-assisted ultrasonic treatment) and γ-TaON (by hydrothermal method followed by nitridation heat treatment) were refluxed in an oil bath at 90 °C for 3 h to develop CQD/γ-TaON heterojunctions.[69] The thermal polymerization was adopted by Wang *et al.*[70] to decorate different weight percentages of CQDs on graphitic carbon nitride sheets at 80 °C. For comparison of photocatalytic performance, they have also synthesized CQD/graphitic carbon nitride composites by a hydrothermal method at 180 °C for 6 h.[70] In the work by Zhang *et al.*,[71] thermal heating at 550 °C was used to synthesize CQD/graphitic carbon nitride composites. The individually synthesized CQDs (by thermal treatment) and graphitic carbon nitride (by thermal treatment) were used to develop CQD/graphitic carbon nitride composites by ultrasonic treatment in the presence of ethanol.[72] Zhang *et al.*[73] have adopted several stages of spot heating induced by ultrasonic cavitation effects from a cell disruptor instrument having power in the range of 50–300 W for 4 h to synthesize CQD/carbon nitride composites. The nitrogen-doped CQDs were synthesized by a hydrothermal method and then decorated on graphitic carbon nitride by a solvent evaporation method.[74] The CQDs were synthesized by a hydrothermal method and then decorated on TiO_2/graphitic carbon nitride heterojunctions by thermal treatment at 85 °C for 5 h.[75]

3. Different types of CQD/semiconductor-based photocatalysts

The schematic illustration of photocatalytic hydrogen production by CQD/semiconductors is shown in Fig. 3(A). In CQD/semiconductor-based nanocomposites, for the increased photocatalytic hydrogen generation activity, CQDs perform two crucial functions. (i) Under UV light illumination, CQDs serve as electron reservoirs to trap photogenerated electrons from the semiconductor's conduction band. This enables the effective separation of electrons and holes and, as a result, increases the photocatalytic hydrogen production activity. (ii) Under visible light illumination, the conjugated CQDs function as photosensitizers similar to organic dyes, sensitising semiconductor-based nanostructures into a visible light-responsive "dyad" structure and donating electrons to the semiconductor's conduction band, resulting in visible light-driven photocatalytic hydrogen production activity.[50] Additionally, the addition of nitrogen, sulphur, phosphor, boron, and other elements to CQDs causes the valence band to shift towards the Fermi energy level (reduction in work function), which speeds up the exchange of electrons (accept or donate) compared to CQDs alone.[25,26]

The coupling with green-synthesized CQDs with semiconductor nanoparticles has also gained interest. Sargin *et al.*[52] have synthesized CQDs by a microwave-assisted method using mushroom, which have a size less than 20 nm, as depicted by the HRTEM results, and it confirmed the decoration of CQDs on TiO_2. They argued that the XPS results of CQDs/TiO_2 depicted the presence of nitrogen and phosphorous as well, which arises from the protein and nucleic acid content of mushroom. When the excitation wavelength was increased, the fluorescence peak emission intensity of CQDs showed a red shift and was found to be greater (506 nm). Nevertheless, the suppression in the fluorescence peak emission intensity was observed for CQDs/TiO_2 due to effective photoinduced charge carrier separation, which will benefit photocatalytic hydrogen production. The CQDs/TiO_2 produced hydrogen of 472 μmol g^{-1} under visible light ($\lambda \geq 420$ nm) while it enhanced to 1458 μmol g^{-1} with the Pt co-catalyst due to the synergistic effects between individual components such as CQDs, TiO_2 and Pt, leading to the transfer of photogenerated electrons from the conduction band (CB) of CQDs to the CB of TiO_2 and then to Pt, which reduced H^+ ions to H_2.

Further, the photocatalytic hydrogen production not only depends on the photocatalysts, but also depends on the content of cocatalysts, pH of solution, incident wavelength and weight of photocatalysts.[54] Fig. 4(A) and (B) depict the spherical shaped CQDs of size 6–7 nm coupled with anatase TiO_2 nanosheet/Pt nanohybrids. The developed CQDs/TiO_2 exhibited hydrogen production ($\lambda = 405$ nm) of 6.2 μmol g^{-1} h^{-1} (Fig. 4(C)), while it increased to 895, 1841, 2106 and 2650 μmol g^{-1} h^{-1} with 0.5%, 1%, 2% and 3% Pt contents respectively, indicating that the presence of co-catalysts such as platinum contributes to increased hydrogen production. The hydrogen production of CQD/1%Pt/TiO_2 nanohybrids with ascorbic acid solutions of various pH is shown in Fig. 4(D). The highest hydrogen production rate of 1867 μmol g^{-1} h^{-1} was found at pH = 4.0 of the ascorbic acid solution with the CQD/1%Pt/TiO_2 photocatalyst, and the pH was found to be negligible before and after mixing with the photocatalysts. Fig. 4(E) displays the dependence on the illumination wavelength for hydrogen production

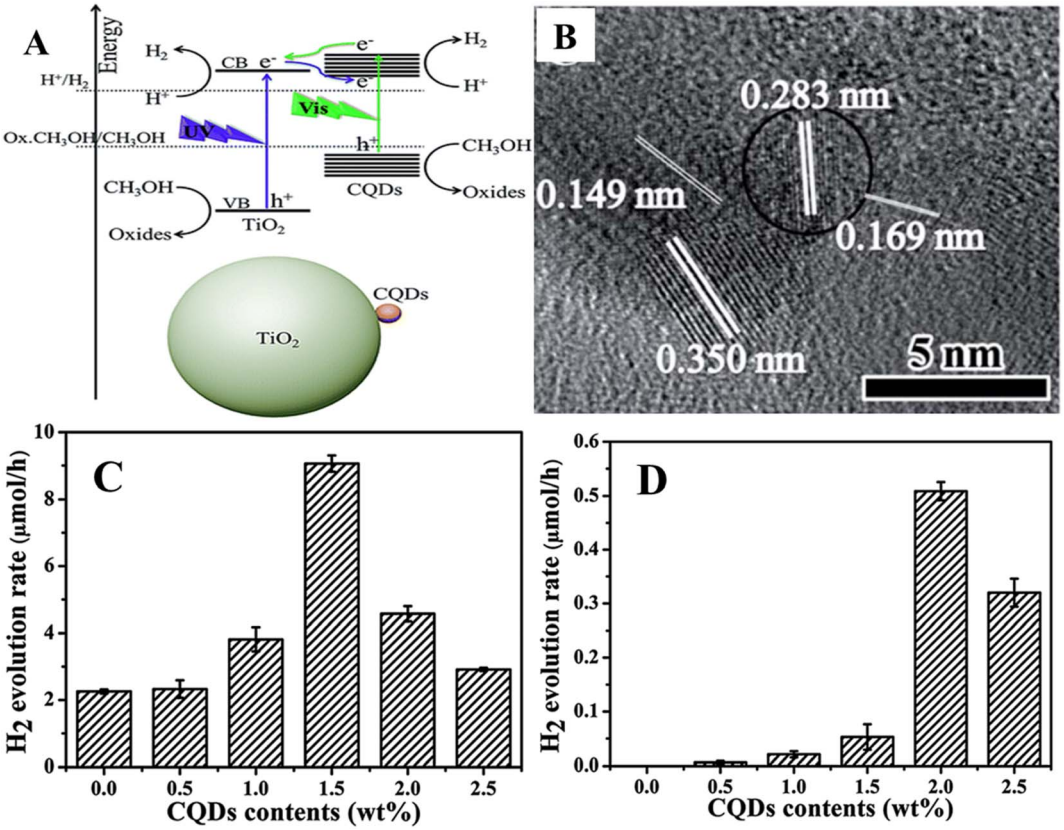

Fig. 3 (A) Schematic of the production of photocatalytic hydrogen using semiconductor (TiO_2)/CQDs when exposed to ultraviolet and visible light. (B) HRTEM image of CQD/TiO_2 nanoparticles, and photocatalytic hydrogen production of CQDs/TiO_2 under (C) UV-visible light and (D) visible light ($\lambda \geq 450$ nm) irradiation. This figure has been reproduced from ref. 50 with permission from the Royal Society of Chemistry, Copyright 2014.

with CQD/1%Pt/TiO_2 photocatalysts, which shows that the hydrogen production was found to be 1525 μmol g^{-1} h^{-1} with illumination at 450 nm and it decreased to 470 μmol g^{-1} h^{-1} with illumination at 520 nm, suggesting that CQDs significantly enhanced the visible light absorption of the photocatalytic system in the visible region. Fig. 4(F) shows the dependence of hydrogen production on the weight of photocatalyst (CQDs/1% Pt/TiO_2) and the highest efficiency was found to be 3323 μmol g^{-1} h^{-1} with 0.125 mg mL^{-1} CQDs/1%Pt/TiO_2. The photon-to-hydrogen conversion efficiency was reduced to 0.57% in the first three hours when the weight of CQDs/1%Pt/TiO_2 was increased to 0.25 mg mL^{-1}, and it was further decreased when the weight was increased to 0.5 mg mL^{-1}. The better interaction between CQDs and TiO_2 facilitating the efficient charge transfer from to TiO_2 from CQDs under visible light illumination was the cause of the enhanced photocatalytic hydrogen production of the nanohybrid. The charge transfer time was found to be 1.3 ns for CQDs/TiO_2, which is comparable to time (1.6 ns) for electron transfer from ascorbic acid to CQDs, suggesting the availability of reductive and oxidative quenching paths for hydrogen production, wherein CQDs act as the electron acceptor and transferring bridge.

The facet of semiconductor coupled with CQDs also plays a role in enhancing the photocatalytic hydrogen production activity. Sui *et al.*[51] have uniformly decorated CQDs of size (2–5) nm on TiO_2-001 nanosheets of average size ~50 nm and thickness of about 4–6 nm with a fringe spacing of 0.235 nm corresponding to the (001) plane of TiO_2-001 (Fig. 5(A)). Fig. 5(B) displays the various TiO_2-001-based photocatalysts used for photocatalytic hydrogen generation. It shows that CQDs/TiO_2-001 produced hydrogen at a rate of 7.9 mol h^{-1}, which is four times higher than that of TiO_2-001 alone. Even CQDs.TiO_2-001 displayed an enhanced hydrogen production rate compared to CQDs/TiO_2 (P25). The improved hydrogen production rate of CQDs/TiO_2-001 is illustrated in Fig. 5(C) and (D). As can be seen in Fig. 5(D), the highly active (001) TiO_2 facet migrates the photoexcited electrons to the TiO_2 surface and combines with H^+ ions forming H_2. Further, CQDs suppress the photoexcited electron–hole pair recombination on the surface of TiO_2-001 favouring the hydrogen production, which is further corroborated by the decrease in lower band–band PL intensity. CQDs serve as electron reservoirs as well as photosensitizers through a new Ti–O–C bond formed between TiO_2-001 and CQDs.

The CQDs decorated on mixed phases of TiO_2 such as anatase and brookite phases of TiO_2 showed an enhanced photocatalytic hydrogen production rate of 280 μmol h^{-1} for 0.5% loading of CQDs.[55] This is due to the absorption edge shift from ultraviolet region to visible region. The CQDs would have

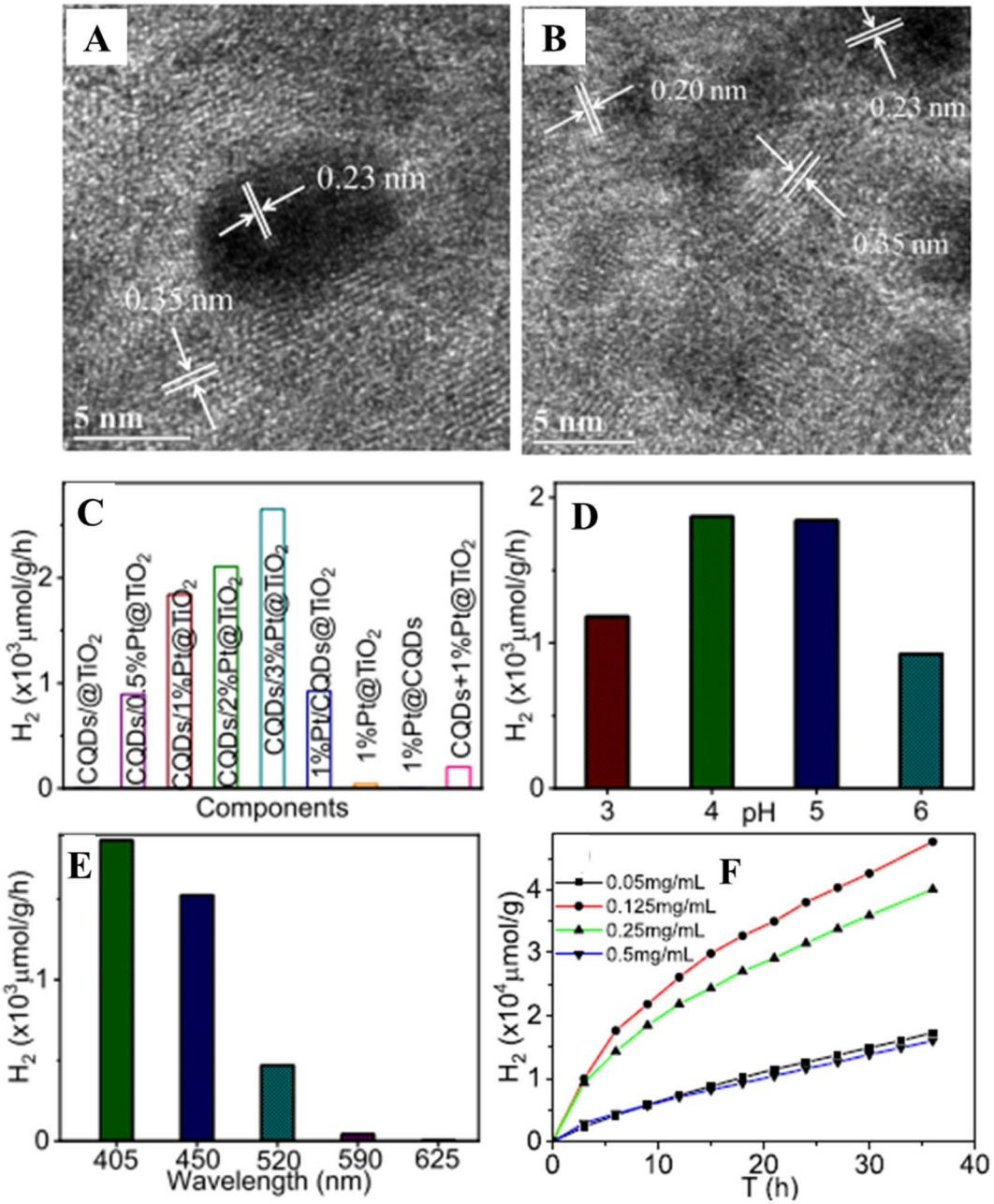

Fig. 4 (A and B) HRTEM images of CQDs/3 wt%Pt/TiO_2. Hydrogen production dependence on (C) photocatalysts, (D) pH, (E) illuminated wavelength and (F) concentration of photocatalyst for CQD/1 wt%Pt/TiO_2 nanohybrids. This figure has been reproduced from ref. 54 with permission from the American Chemical Society, Copyright 2019.

formed good contact interface with surface TiO_2 *via* a Ti–O–C bond introducing defects such as Ti^{3+}/oxygen vacancies and provided the surface with hydrogenation-reduced CQDs, which in turn varies the wavelength absorption as well as emission properties. Due to this hydrogenation, the CQDs will lose their surface groups, leading to an increase in the degree of conjugation, resulting in electron transfer from CQDs to TiO_2, thereby decreasing the band gap (*i.e.*, a red shift in the absorption band edge).[55] The biomass-originated carbon dots of size around (3–4) nm were decorated onto anatase-phase TiO_2 nanoparticles.[56] The CDs/TiO_2 showed an enhanced photocatalytic hydrogen production rate of 603.92 μmol h^{-1} g^{-1}, which was 6.41-fold higher than that of TiO_2 alone (*i.e.* 94.18 μmol h^{-1} g^{-1}). This enhancement in hydrogen production was mainly due to the decoration of CDs on TiO_2 resulting in the formation of Ti–O–C leading to easy transfer of electrons from CDs to TiO_2. Even the photocatalyst exhibited remarkable hydrogen production cyclic stability over 20 h and found no change in its structural and chemical properties. As the CDs transfer electrons to TiO_2, it leads to the huge accumulation of charges at the interface of CDs/TiO_2, resulting in the electric field distribution at the interface.[56] Moreover, they have carried

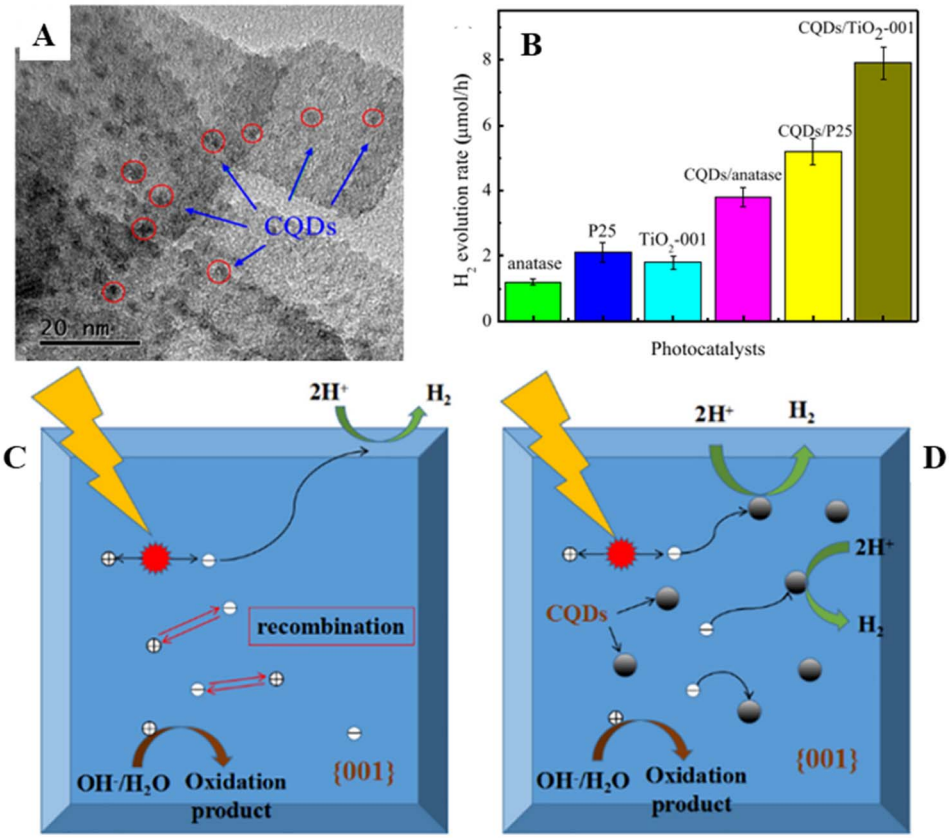

Fig. 5 (A) HRTEM image of CQDs/TiO_2-001. (B) Photocatalytic hydrogen production of different photocatalysts based on TiO_2-001. Illustration of charge transfer mechanisms and hydrogen production of (C) TiO_2-001 and (D) CQDs/TiO_2-001. This figure has been reproduced from ref. 51 with permission from Elsevier, Copyright 2019.

out Finite-difference time-domain (FDTD) simulations to study the electric field distribution at the interface of CDs/TiO_2, as shown in Fig. 6. As shown in Fig. 6(A), when wavelength 550 nm was incident, the local "hot spots" were observed at the TiO_2 interface, suggesting the huge accumulation of charge carriers in these regions. When the same wavelength (550 nm) was incident, locally enhanced "hot spots" were identified at the TiO_2 and CD interface, suggesting the huge accumulation of charge carriers at the interface of TiO_2 and CDs. Moreover, the electric field intensity was found to be significantly more for CDs/TiO_2, confirming the transfer of charges across the interface. This suggests that the enhancement in the photocatalytic production of hydrogen CDs/TiO_2 was because of the synergistic effects multiple mechanisms, such as enhancement in the optical absorption and separation of photogenerated charge carriers along with the promotion of photogenerated electron transfer.

The CQDs were also coupled with metal chalcogenides to enhance their photocatalytic hydrogen production. The CQDs decorated on MoS_2 nanoplates were self-assembled on $ZnIn_2S_4$ nanosheets by Wang *et al.*[57] The hydrogen produced was negligible for MoS_2/CQDs, and bare $ZnIn_2S_4$ showed poor photocatalytic hydrogen production. However, 3 wt% MoS_2/CQDs/$ZnIn_2S_4$ demonstrated 674 μmol hydrogen production over 5 h, which was 2 and 5.1 times greater than that of 3 wt% MoS_2/$ZnIn_2S_4$ and 3 wt% CQDs/$ZnIn_2S_4$ correspondingly. The addition of CQDs during the fabrication of ternary nanocomposites considerably increased the photocatalytic hydrogen production activity of the material, which is advantageous for the vectorial transport of photogenerated electrons from $ZnIn_2S_4$ to MoS_2. $ZnIn_2S_4$ produces electrons and holes when the ternary nanocomposite is irradiated by light. These photogenerated electrons are transferred to CB of CQDs as the CB of CQDs is less negative compared to that of $ZnIn_2S_4$. As the conductivity of CQDs is good, these photogenerated electrons can then be transferred to MoS_2 providing active sites for the production of hydrogen. The effective transfer of electrons from $ZnIn_2S_4$ to MoS_2 is influenced by CQDs, which act as mediators. The spherically shaped CQDs of size 4–9 nm were decorated on micron-sized $KNbO_3$ particles by Qu *et al.*[58] The CQD/$KNbO_3$ composite showed an enhanced photocatalytic hydrogen production of 468.72 μmol h^{-1} g^{-1} while bare $KNbO_3$ showed 245.52 μmol h^{-1} g^{-1} due to the suppression in the recombination of photogenerated electron hole pairs. The photogenerated electrons in $KNbO_3$ are transferred to CQDs, which provides active sites for hydrogen production, thereby decreasing the recombination of electron–hole pairs. Further, the absorption and fluorescence properties of CQDs can be enhanced by doping[20–24] as well as co-doping[25–28] with non-metal elements, which enhance the photocatalytic hydrogen

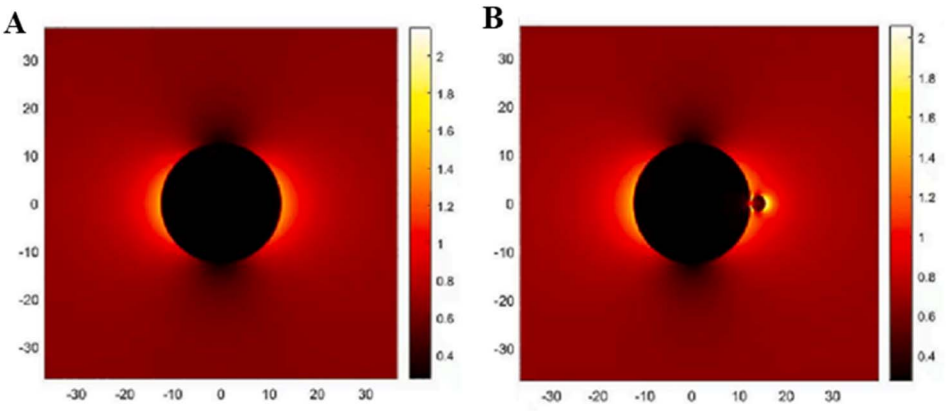

Fig. 6 Electric field distribution calculated from FDTD simulations for (A) TiO_2 and (B) CDs/TiO_2. The electric field's direction was polarised along the *X*-axis before incidentally intersecting the *Z*-axis. This figure has been reproduced from ref. 56 with permission from Elsevier, Copyright 2023.

production of CQD/semiconductor photocatalysts. Shi *et al.*[76] have investigated the effect of nitrogen doping level in NCQDs/TiO_2 for photocatalytic hydrogen production. The hydrogen production rate was 9.8 μmol h^{-1} for NCQDs/TiO_2 under full-spectrum illumination, which is ~9 times higher than that of TiO_2 alone. Under visible light illumination ($\lambda \geq 450$ nm), the NCQDs/TiO_2 exhibited 58.6 nmol h^{-1}, whereas pristine TiO_2 showed no hydrogen production. It is evident that NCQDs are beneficial for hydrogen production under both full spectrum and visible light illumination. They concluded that NCQDs serve as both photosensitizers and electron reservoirs in NCQD/TiO_2 composites. Nitrogen doping supresses non-radiative quenching by decreasing the inner layer energy traps between sp^2 domains, in turn leading to a high PLQY. Under UV light illumination, NCQDs accept the photoexcited electrons from TiO_2 and under visible light illumination, NQCDs donate the photoexcited electrons to TiO_2, thereby enhancing the hydrogen production under full-spectrum illumination. Yashwanth *et al.*[25] have co-doped nitrogen and phosphorus to CQDs (NPCQDs) of size (1–5) nm and then decorated NPCQDs on anatase-phase TiO_2 nanoparticles of size 7–15 nm. NPCQDs/TiO_2 showed improved photocatalytic hydrogen production of 533 μmol h^{-1} g^{-1} as compared to NCQDs/TiO_2, PCQDs/TiO_2, and CQDs/TiO_2. This is due to the synergistic effects between individual components leading to a decrease in band gap, supressed recombination of photoexcited electron–hole pairs, increased lifetime of photoexcited charge carriers and decreased work function. The nitrogen as well as phosphorous co-dopants create an additional energy level above the VB of CQDs, leading to shifting of the Fermi energy level towards the CB, resulting in the transfer of more electrons from NPCQDs to TiO_2. This would create virtual energy levels (acceptor energy levels) below the conduction band of TiO_2, resulting in a decrease in the band gap of NPCQDs/TiO_2. Hence, NPCQDs/TiO_2 will be more active in the visible region for the production of photocatalytic hydrogen. The observed more hydrogen production by PCQDs/TiO_2 than NCQDs/TiO_2 is due to the longer lifetime of energy levels produced by phosphor dopants. The NPCQDs of size (2–5) nm were decorated onto hexagonal wurtzite-structured ZnO nanorods with a diameter of 25–40 nm and a length of ~70 nm.[26] The NPCQDs/ZnO showed an increased photocatalytic hydrogen rate of 417 μmol h^{-1} g^{-1} compared to PCQDs/ZnO, NCQDs/ZnO and CQDs/ZnO due to the effective transfer of photogenerated electrons from NPCQDs to TiO_2, thereby supressing the recombination of photogenerated electron–hole pairs with the extended lifetime of photogenerated charge carriers. Xu *et al.*[77] have co-doped nitrogen and sulphur to CQDs (NSCQDs) with an average size of 2.71 nm and decorated on a cobalt-based metal organic frame (Co-MOF) surface and graphitic carbon nitride (CN). Relatively Co-MOFs and CN have very low photocatalytic hydrogen production activities. Nevertheless, 15NSCQDs/Co-MOF/0.125CN showed enhanced photocatalytic hydrogen production of 312.65 μmol over 5 hours. They argued that under visible light illumination, the Co-MOF/CN acts as a Z-type heterojunction, wherein photogenerated electrons of CN are transferred to the VB of the Co-MOF and recombine with holes, resulting in the suppressed hydrogen production. Nevertheless, the introduced CQD serves as an electron bin and acts as an electron transporter in the photocatalyst. Part of the photogenerated electrons of CN are transferred to NSCQDs, which produces hydrogen on its surface. The remaining part of photogenerated electrons of CN are transferred to NSCQDs, which then transfer those electrons to the CB of the Co-MOF, which provides active sites for hydrogen production. Thus, NSCQDs supress photogenerated electron–hole pair recombination and also act as a bridge to transfer the photogenerated electrons, enhancing the photocatalytic hydrogen production of NSCQD/Co-MOF/CN composites. Further, very recent studies have demonstrated that the coal-based carbon quantum dots enhanced the photocatalytic hydrogen production rate of $CoMoO_4$/g-C_3N_4 to 4916.63 μmol g^{-1} h^{-1} as the CQD serves as a bridge between $CoMoO_4$ and g-C_3N_4 due to its excellent electron transfer capabilities of serving as the electron acceptor as well as electron donor.[62] Moreover, the coal-based nitrogen, sulfur-rich CQDs increased the photocatalytic hydrogen production rate of Co–Fe–P derived from the MOF to 28.41 mmol g^{-1} h^{-1}, and CQDs served as auxiliary catalysts to

boost the hydrogen production.[63] Patra *et al.*[66] have dispersed CQDs of size ~2–7 nm on the $BaZrO_{3-\delta}$ hollow sphere. The developed CQD/$BaZrO_{3-\delta}$ heterostructure showed enhanced hydrogen production rates of 670 μmol h^{-1} g^{-1} and 250 μmol h^{-1} g^{-1} under ultraviolet and visible light irradiation respectively compared to the $BaZrO_{3-\delta}$ hollow sphere alone. The enhanced hydrogen production of the CQD/$BaZrO_{3-\delta}$ heterostructure was due to the dual nature of CQDs as electron acceptors and electron donors under ultraviolet and visible light irradiation respectively, as explained in Fig. 7(A). Gogoi *et al.*[67] have decorated different weight percentages of CQDs on 1D CdS nanorods of diameter ~30 nm and average length 2–4 nm to enhance photocatalytic hydrogen production. The highest photocatalytic hydrogen production of 309 mmol h^{-1} g^{-1} was achieved for 0.4 wt% CQD/CdS composite, which was 1.5 times higher than that of CdS alone. The enhanced hydrogen production was due to the strong interaction between CQDs and CdS, resulting in the negative shift of binding energies of Cd 3d and S 2p, which confirmed the increase in the density of states. This will enable the fast transfer of photoexcited electrons from CQDs to CdS and then increase the photocatalytic hydrogen production efficiency. Further, the charge separation efficiency of CQDs/CdS was studied by chronoamperometry (Fig. 7(B)), and it showed a higher average current density for CQDs/CdS compared to CdS due to the photo quantum confinement effect of CQDs helping the easy transfer of photo excited electrons from CQDs to CdS. Moreover, the reduction in the arc radius of EIS spectra (Fig. 7(C)) for composite under visible light was due to the faster transfer of photoexcited electrons. The amount of CQD/CdS photocatalyst was also optimized, which showed better photocatalytic efficiency at 1 mg L^{-1} and decreased thereafter (Fig. 7(E)). The higher loading of the photocatalyst make the solution turbid and block the light, thereby decreasing the efficiency of photocatalytic hydrogen.

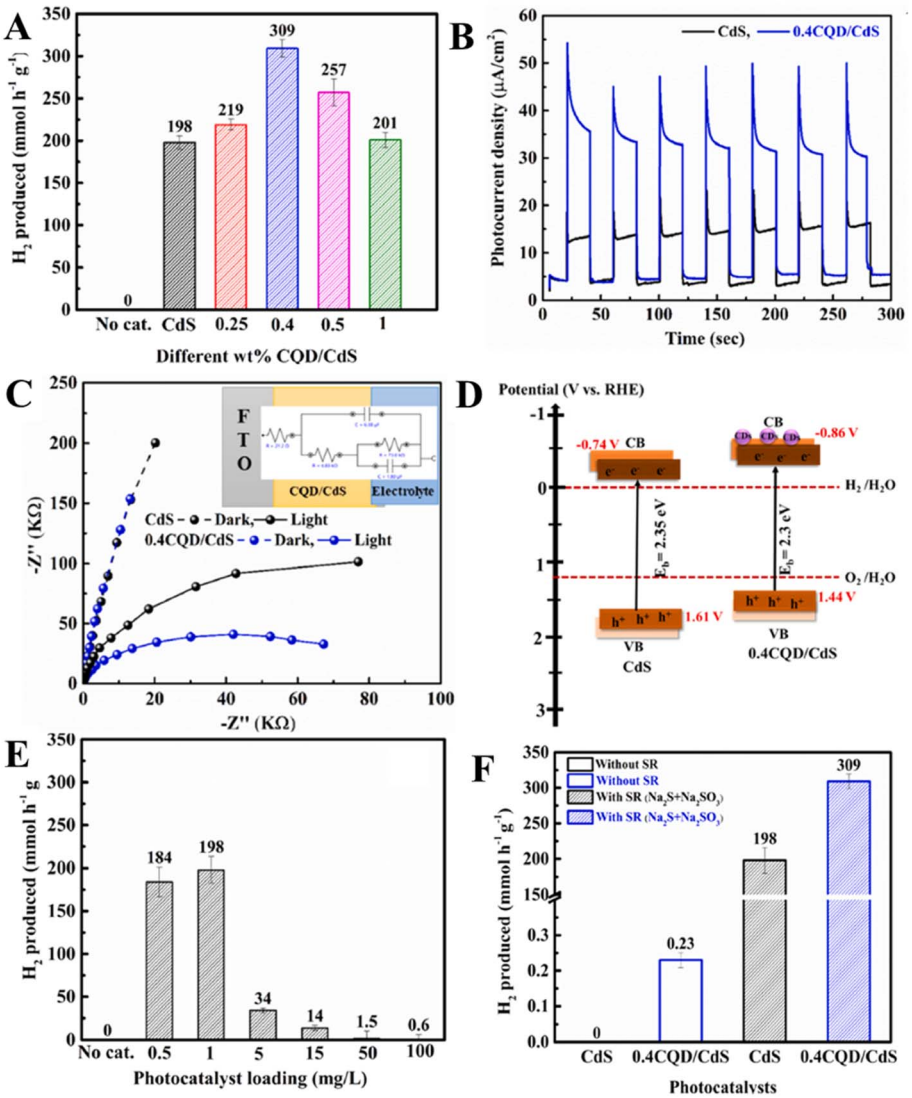

Fig. 7 (A) Photocatalytic hydrogen production using different photocatalysts. (B) Transient photocurrent curves, (C) EIS spectra, (D) energy band diagram, (E) effect of photocatalyst loading, and (F) effect of sacrificial reagents on photocatalytic hydrogen production of CQD/CdS composites. This figure has been reproduced from ref. 67 with permission from Elsevier, Copyright 2020.

Further, the CQDs provide the oxidation/reduction active sites to CdS in the absence of sacrificial reagents, thereby enhancing the photocatalytic hydrogen activity (Fig. 7(F)), and also protect the photocorrosion of CdS under light irradiation.

CQDs were also used to boost the photocatalytic hydrogen production of binary composites such as $LaFeO_3$/CdS. Ternary composites such as $LaFeO_3$/CdS/CQDs exhibited an enhanced hydrogen production rate of 25 302 μmol h^{-1} g^{-1}, which is 1.1 times higher than that of LaFeO/CdS binary composites. The decorated CQDs act as mediators to harvest the sunlight and enhance the photoinduced charge carrier separation to boost the photocatalytic hydrogen production. Furthermore, CQDs receive the electron from $LaFeO_3$ and reduces H^+ to H_2, whereas the holes in the valence band of CdS oxidize lactic acid to pyruvic acid.[68] Hou *et al.*[69] have decorated the CQDs of size 2–5 nm on γ-TaON hollow urchins consisting of well-organized nanoneedles of length 100–200 nm (Fig. 8(A)–(C)). The developed CQD/γ-TaON heterostructures exhibited a hydrogen production rate of 496.5 μmol h^{-1}, which is 1.25 times higher than that of γ-TaON (Fig. 8(D)). The detailed photocatalytic hydrogen production mechanism of CQD/γ-TaON is shown in Fig. 8(E). The CQDs receive electrons from γ-TaON and transport them to photocatalytic processes under UV-visible light, thereby preventing the electron–hole recombination, which further enhances the photocatalytic hydrogen production by CQD/γ-TaON heterostructures. Under NIR light irradiation, CQDs absorb longer wavelength light and emit shorter wavelength light due to the up-conversion behaviour, which further excites γ-TaON to produce electron–hole pairs, harnessing the broad spectrum of sunlight to produce hydrogen effectively. Even the developed CQD/γ-TaON heterostructure depicted excellent stability for photocatalytic hydrogen production for over 30 h, revealing its high durability as a photocatalyst. The CQDs/γ-TaON showed 12.2% quantum efficiency, which is 61 times higher than that of conventional TaON.[69]

The thermal polymerization was used to develop CQD/graphitic carbon nitride composite-based photocatalysts for hydrogen production.[70] The schematic of the synthesis of CQD/graphitic carbon nitride composites along with the proposed photocatalytic hydrogen production mechanism is shown in Fig. 9. During the synthesis, the precursors of CQDs and graphitic carbon nitride such as glucose and urea respectively recrystallize and form hydrogen bonding between the hydroxyl groups of glucose and the amide groups of urea. During thermal polymerization, urea polymerizes to graphitic carbon nitride and glucose carbonizes to CQDs. As there will be a hydrogen bonding between glucose and urea, it creates close connections (may be van der Waals' type of force/bond) between CQDs and graphitic carbon nitride, which could enhance the charge transfer process and prevent the recombination of electron–hole pairs at the interface. As a result, the CQD/graphitic carbon nitride composite showed enhanced photocatalytic hydrogen production of ~465 μmol, which is 4.55 times higher than that of graphitic carbon nitride alone. Furthermore, CQD/graphitic carbon nitride composites prepared by thermal polymerization showed enhanced photocatalytic hydrogen production under the same conditions compared to CQD/graphitic carbon nitride composites prepared by a hydrothermal method. This is due to the reason as explained earlier that the presence of hydrogen bonding between glucose and urea establishes the close connection (may be van der Waals' type of force/bond) between CQDs and graphitic carbon nitride, thereby enhancing the electron transfer across the interface, which, in turn, increases the photocatalytic hydrogen production of CQDs/graphitic carbon nitride prepared by a thermal polymerization method. Zhang *et al.*[71] have also developed CQDs/graphitic carbon nitride and found that the band gap decreased to 2.68 eV for CQDs/graphitic carbon nitride from 2.77 eV for graphitic carbon nitride alone. Under visible light irradiation, the photoexcited electrons and holes will generate

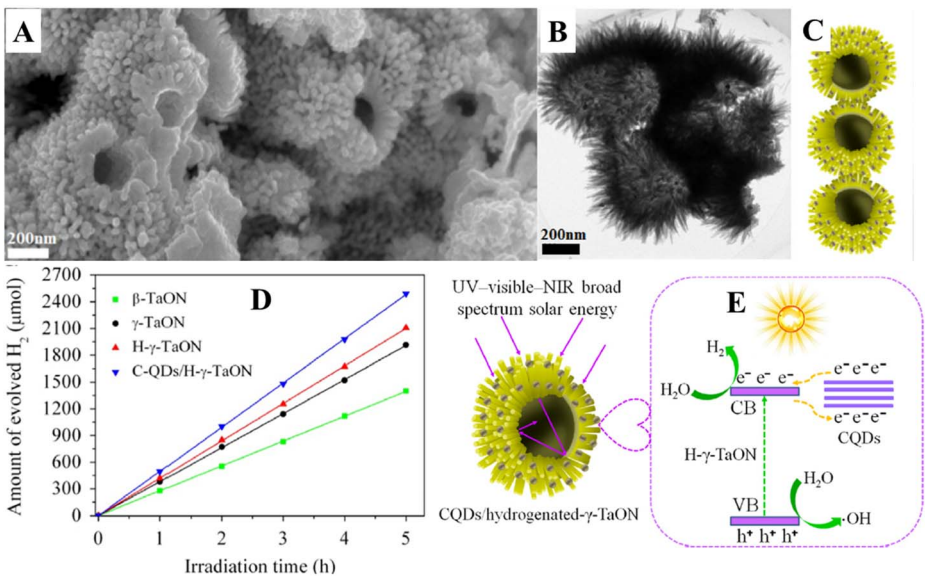

Fig. 8 (A) FESEM image, (B) TEM image, (C) schematic illustration, (D) photocatalytic hydrogen production and (E) schematic photocatalytic mechanism of CQD/γ-TaON heterojunctions. This figure has been reproduced from ref. 69 with permission from Elsevier, Copyright 2015.

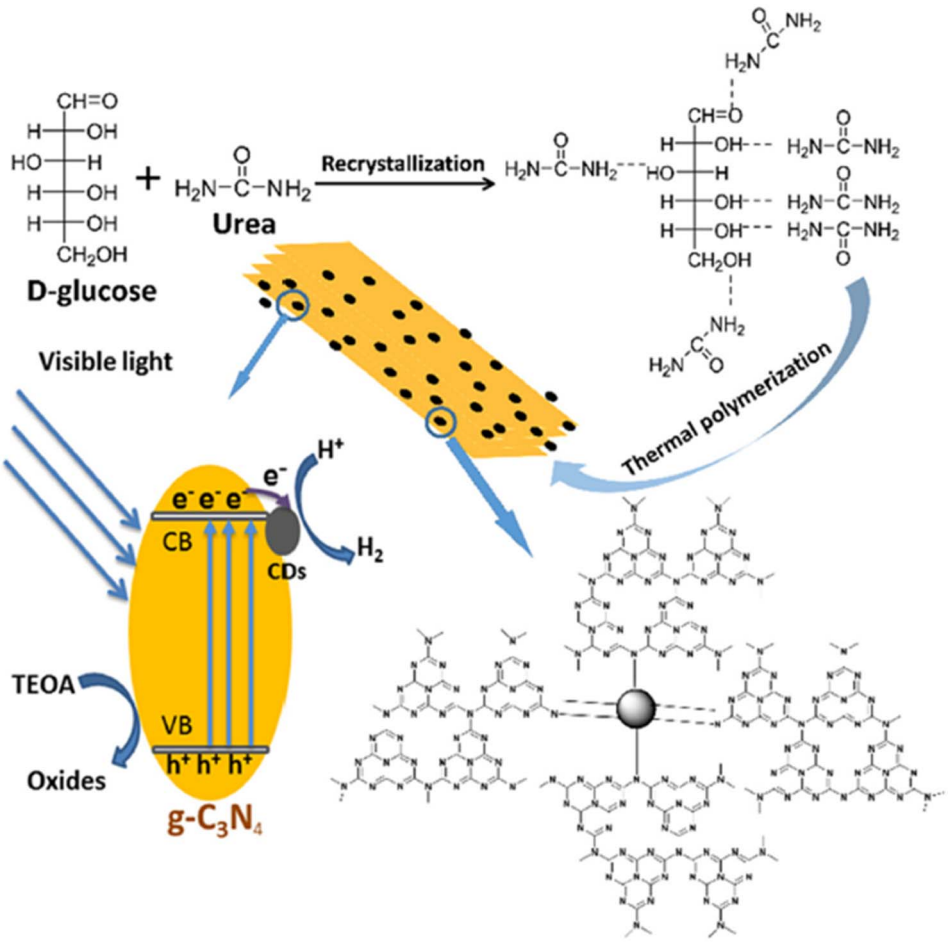

Fig. 9 Schematic of the synthesis and photocatalytic hydrogen production of CQD/graphitic carbon nitride composites. This figure has been reproduced from ref. 70 with permission from Elsevier, Copyright 2018.

graphitic carbon nitride and create an internal electric field within it. This was further corroborated by first-principles DFT calculations, depicting the local electronic structure in the composite and also indicating the strong hybridization between CQDs and graphitic carbon nitride, which leads to the creation of internal electric field. The photogenerated electrons from graphitic carbon nitride will quickly transfer to CQDs and the photogenerated holes will remain on graphitic carbon nitride forming the spatial separation degrading Rhodamine B. As a result, CQDs/graphitic carbon nitride composite exhibited a hydrogen production rate of 1291 μmol g^{-1} h^{-1} simultaneously degrading rhodamine B. The produced hydrogen was 1.94 times higher than that of the same CQD/graphitic carbon nitride photocatalyst in water. It summarizes that the efficient utilization of holes to degrade rhodamine B prevents the fast recombination of photogenerated electrons and holes, thereby enhancing the photocatalytic hydrogen production. Li *et al.*[72] have modified the graphitic carbon nitride sheets using CQDs of size 2–10 nm. The CQD/graphitic carbon nitride composite showed an enhanced photocatalytic hydrogen production rate of 116.1 μmol h^{-1} which is three times higher than that of graphitic carbon nitride alone. The enhancement in the photocatalytic hydrogen production was attributed to the fact that the CQDs serve as electron reservoirs and also act as light harvesters, thereby increasing the photocatalytic hydrogen production by CQD/graphitic carbon nitride composites.

The CQDs of size ~2 nm were loaded onto a 2D carbon nitride matrix of lateral dimension up to several microns developed by a facile "spot heating" method using an ultrasonicator.[73] During ultrasonic treatment, the exfoliation of bulk carbon nitride occurs, resulting in an increase in interlayer spacing. Simultaneously, some regions of ultrathin carbon nitride decompose into nitrogen/cyano fragments by the high temperature due to the intensified ultrasonic cavitation effect leaving behind the carbon atoms at their original site, thus forming CQDs in the 2D carbon nitride matrix. With the increase in ultrasonic power, the amount of CQDs on carbon nitride sheets also increased. The photocatalytic hydrogen production of the developed CQD/carbon nitride matrix was characterized as a function of irradiation time by a solid-state magic angle spinning nuclear magnetic resonance technique in the organic contaminated water in the presence and absence of bisphenol A. The amount of hydrogen produced increased with the increase in time and was found to be more for the CQD/

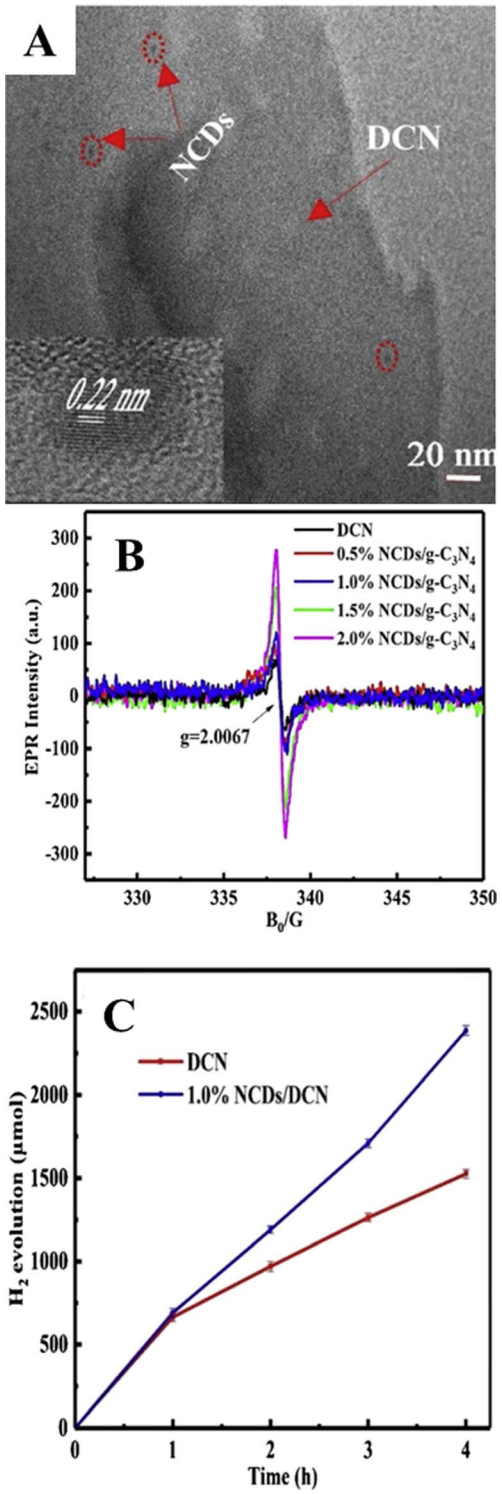

Fig. 10 (A) TEM image of 1% CQDs/graphitic carbon nitride (inset shows its lattice spacing). (B) electron spin resonance of CQDs/graphitic carbon nitride, (C) hydrogen evolution of 1% CQDs/graphitic carbon nitride. This figure has been reproduced from ref. 74 with the permission from Elsevier, Copyright 2020.

carbon nitride photocatalyst than that of individual carbon nitride. The amount of hydrogen produced by CQDs/carbon nitride matrix was found to be more as 152 μmol g^{-1} h^{-1} due to the increased lifetime of photogenerated charge carriers as well as synergistic effects between water splitting and bisphenol-A degradation.

Further, Liu *et al.*[74] have doped CQDs with nitrogen to enhance the hydrogen evolution of nitrogen-doped CQD-decorated defect-rich graphitic carbon nitride (Fig. 10(A)). The electron spin resonance spectra showed a progressive increase in spin intensity with the increase in CQD amount (Fig. 10(B)), indicating the promoted delocalization of the sole electrons, which is due to the improved charge separation and effective migration of charge carriers in NCQD/graphitic carbon nitride composites. The 1% CQD-loaded graphitic carbon nitride composite showed the highest hydrogen production rate of 626.93 μmol g^{-1} h^{-1} (Fig. 10(C)) which is nearly 7 times higher than that of graphitic carbon nitride alone due to increased photogenerated charge separation, increased lifetime of photogenerated charge carriers and increased specific surface area. In addition, the lone pair of electrons in the amine groups of nitrogen atoms interact with the photogenerated holes, resulting in an increased lifetime of photogenerated electrons, which will be utilized to combine with H^+ to produce hydrogen. The tertiary composite consisting of CQD-decorated TiO_2 nanoparticle/2D graphitic carbon nitride heterojunctions (CQDs-TiO_2-C_3N_4) was developed that produced hydrogen of nearly 6.497 μmol g^{-1} h^{-1} which is nearly two times higher than that of C_3N_4 alone.[75] Pan *et al.* have proposed a mechanism for photocatalytic hydrogen production, as shown in Fig. 11. Under visible light as well as near-ultraviolet light irradiation, CQDs showed up-conversion fluorescence through a two-photon process. As a result, part of visible light will get converted into ultraviolet light and excite the electrons in TiO_2 generating photoexcited charge carriers. Further, heterojunctions such as TiO_2–C_3N_4 increase the lifetime of photogenerated charge carriers in addition to the decomposition of H_2O_2 by CQDs, and the four-electron process can be described as follows:

$$H_2O \rightarrow H_2 + \frac{1}{2}O_2 \quad (7)$$

$$2H_2O \rightarrow H_2O_2 + H_2 \quad (8)$$

$$H_2O_2 \rightarrow H_2O + \frac{1}{2}O_2 \quad (9)$$

C_3N_4 in the tertiary composite acts as a hole acceptor and produces H_2O_2 on the surface of photocatalysts. The CQDs on the surface of TiO_2/C_3N_4 heterojunctions decompose H_2O_2 into H_2O with evolution of oxygen, as shown in eqn (9). Thus produced H_2O will release hydrogen, as shown in eqn (7) by the photogenerated electrons of TiO_2. Furthermore, C_3N_4 produces a porous structure, thereby enhancing the specific surface area to provide the active sites for hydrogen production. The synergistic effects of all these enhance the photocatalytic hydrogen production activity of CQD-TiO_2-C_3N_4 tertiary composites compared to other binary as well as individual components. The comparison of different CQD/semiconductor-based photocatalysts with their hydrogen production is tabulated in Table 1.

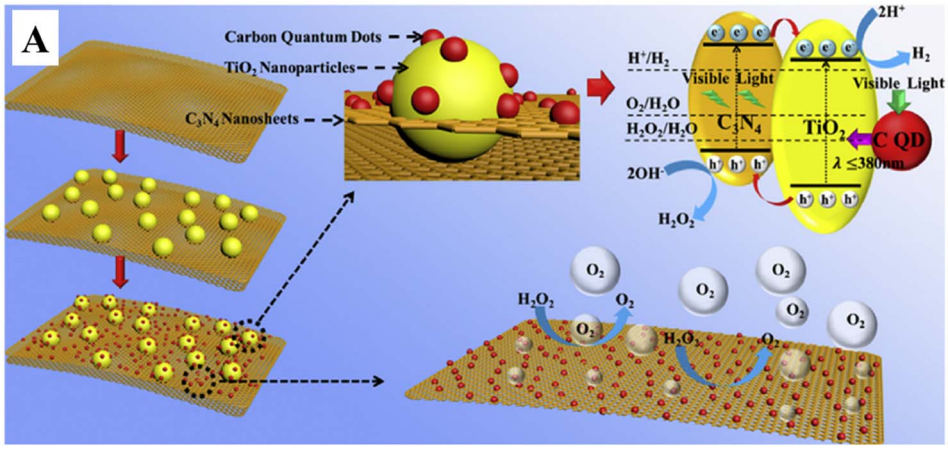

Fig. 11 (A) Schematic of the photocatalytic hydrogen production activity of the CQD-TiO_2-C_3N_4 tertiary composite. This figure has been reproduced from ref. 75 with permission from Elsevier, Copyright 2018.

Table 1 Comparison of different photocatalysts with their hydrogen production

Sl. No.	Photocatalyst	Source	H_2 produced	Reference
1	CQDs/TiO_2 nanoparticle	500 W halogen lamp (UV light)	9.1 μmol h^{-1}	50
2	CQDs/TiO_2 nanoparticle	500 W halogen lamp (λ > 450 nm)	0.5 μmol h^{-1}	50
3	CQDs/TiO_2 nanosheets	300 W xenon lamp	7.9 μmol h^{-1}	51
4	CQDs/TiO_2 nanoparticles	300 W xenon lamp ($\lambda \geq$ 420 nm)	472 μmol h^{-1} g^{-1}	52
5	CQDs/TiO_2/Pt	300 W xenon lamp ($\lambda \geq$ 420 nm)	1458 μmol h^{-1} g^{-1}	52
6	CQDs/TiO_2/Pt	LED lamp (λ = 405 nm)	1867 μmol g^{-1} h^{-1}	54
7	CQDs/TiO_2	1.5 solar simulator (AM 1.5 filter)	280 μmol h^{-1}	55
8	CQDs/TiO_2	300 W xenon lamp (AM 1.5)	603.92 μmol h^{-1} g^{-1}	56
9	MoS_2/CQDs/$ZnIn_2S_4$	300 W xenon lamp ($\lambda \geq$ 420 nm)	674 μmol	57
10	CQDs/$KNbO_3$	300 W xenon lamp (420 nm < λ < 800 nm)	468.72 μmol h^{-1} g^{-1}	58
11	NCQDs/TiO_2	500 W metal halide lamp ($\lambda \geq$ 450 nm)	58.6 nmol h^{-1}	76
12	NPCQDs/TiO_2	300 W xenon lamp ($\lambda \geq$ 410 nm)	533 nmol h^{-1} g^{-1}	25
13	NSCQDs/CoMoF	5 W LED lamp	312.65 μmol	77
14	CQDs/$CoMoO_4$/graphitic carbon nitride	5 W LED lamp ($\lambda \geq$ 420 nm)	4916.63 μmol g^{-1} h^{-1}	62
15	NSCQDs/CoFeP	5 W LED lamp ($\lambda \geq$ 420 nm)	28.41 mmol g^{-1} h^{-1}	63
16	NPCQDs/ZnO	300 W xenon lamp ($\lambda \geq$ 410 nm)	417 nmol h^{-1} g^{-1}	26
17	CQDs/$BaZrO_{3-\delta}$	300 W tungsten-halogen lamp	670 μmol h^{-1} g^{-1}	66
18	CQDs/CdS nanowires	400 W metal halide lamp	309 mmol h^{-1} g^{-1}	67
19	$LaFeO_3$/CdS/CQDs	Sun light	25 302 μmol h^{-1} g^{-1}	68
20	CQDs/H-γ-TaON hollow urchins	350 W mercury lamp	496.5 μmol h^{-1}	69
21	CQDs/graphitic carbon nitride	300 W xenon lamp	~465 μmol	70
22	CQDs/graphitic carbon nitride	300 W xenon lamp	1291 μmol g^{-1} h^{-1}	71
23	CQDs/graphitic carbon nitride	300 W xenon lamp ($\lambda \geq$ 420 nm)	116.1 μmol h^{-1}	72
24	CQDs/graphitic carbon nitride	AM 1.5 solar power system ($\lambda \geq$ 420 nm)	152 μmol g^{-1} h^{-1}	73
25	NCQDs/graphitic carbon nitride	300 W xenon lamp (λ > 420 nm)	626.93 μmol g^{-1} h^{-1}	74
26	CQDs-TiO_2-C_3N_4	300 W xenon lamp (λ > 400 nm)	6.497 μmol g^{-1} h^{-1}	75

In spite of all these advantages, the CQD-based photocatalyst faces some challenges, which are discussed in the next section.

Further, there are many other photocatalysts that have been developed apart from CQD/semiconductor-based photocatalysts. The ternary composite composed of black phosphorous/Ti_3C_2 MXene/MBene heterojunctions was developed by Zhu *et al.*[78] The TEM (Fig. 12(A)) and HRTEM (Fig. 12(B)) images showed smooth and irregular edges, and demonstrate the presence of black phosphorus, Ti_3C_2 and MBene in tertiary nanocomposites. The tertiary black phosphorous/Ti_3C_2/MBene depicted a hydrogen production rate of 8623.5 μmol g^{-1} h^{-1} which was 15.63, 2.57 and 1.43 times higher than that of black phosphorous, black phosphorous/Ti_3C_2 and black phosphorous/MBene respectively. The wavelength-dependent hydrogen production by tertiary black phosphorous/Ti_3C_2/MBene nanocomposites is shown in Fig. 12(D). The tertiary nanocomposite showed hydrogen production predominantly in the visible region and also in the near-infrared region, showcasing its efficient utilization as a hydrogen production photocatalyst.

The defect-engineered tri-coordinated nitrogen vacancy-modified graphitic carbon nitride showed a photocatalytic

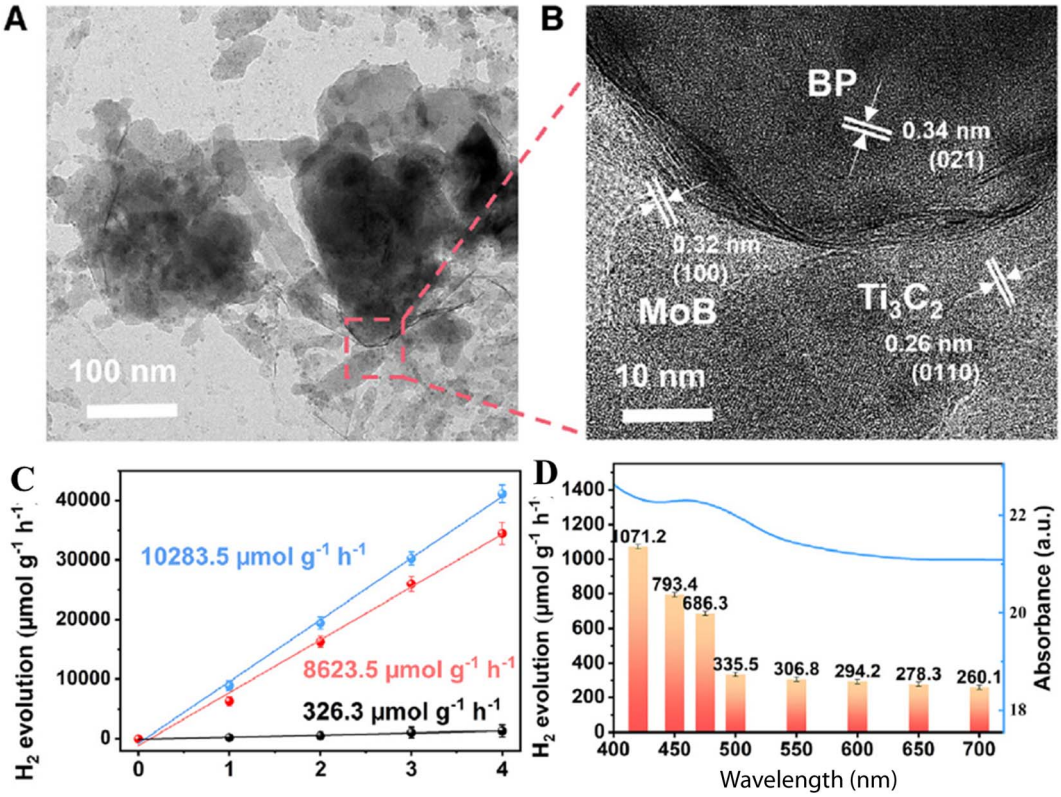

Fig. 12 (A) TEM image, (B) HRTEM image, (C) hydrogen production (red line = $\lambda \geq 420$ nm; blue line = full spectrum; black line = near IR) and (D) wavelength-dependent photocatalytic hydrogen production of the black phosphorous/Ti_3C_2/MBene tertiary nanocomposite. This figure has been reproduced from ref. 78 with permission from Elsevier, Copyright 2024.

hydrogen production rate of 5.45 mmol g^{-1} h^{-1}, which was 7.89 times higher than that of pristine graphitic carbon nitride.[79] The nitrogen vacancies create defect levels below the conduction band of graphitic carbon nitride shortening the distance for photogenerated charge carriers, thereby increasing the photocatalytic hydrogen production. Moreover, these intermediate defect levels absorb H* reducing the Gibbs free energy for photocatalytic hydrogen production and also created an electric field on melon chains, thereby accelerating the charge transfer process, which in turn enhances the photocatalytic hydrogen production.[79] Hyeon *et al.*[80] have developed a floatable nanocomposite which can produce hydrogen of 163 mmol h^{-1} m^{-2} when embedded in Pt/TiO_2 in comparison to 77.2 mmol h^{-1} m^{-2} when submerged in Cu/TiO_2 nanocomposites.[81] Takanabe *et al.*[82] have developed Al-doped $SrTiO_3$ decorated with TiO_x and TaO_x membranes having a thickness < 3 nm. The results demonstrated the high-pressure tolerant vapor-fed photocatalytic water splitting using developed photocatalysts for efficient, durable and scalable hydrogen production.[83] Hydrogenated TiO_2 was developed using wet chemistry strategies with switchable controlled defects, showcasing high photocatalytic hydrogen production.[84] The developed hydrogenated TiO_2 produced hydrogen of 142.9 μmol h^{-1} under UV-visible light which is 60 times higher than that of C-rutile TiO_2. The experimental results along with the theoretical results revealed that the improvement in photocatalytic hydrogen production of hydrogenated TiO_2 was due to the modified electronic structure and band structure of TiO_2.[84,85] Kosco *et al.*[86] have developed two separate organic semiconductor-based heterojunction nanoparticles composed of donor polymer PBDB-T-2F (PM6) with either the narrow band gap non-fullerene acceptor BTP-4F (Y6) or fullerene[6]-phenyl C71 butyric acid methyl ester (PCBM). The efficient separation of exciton takes place at the donor–acceptor heterojunction within the nanoparticle, resulting in the extended lifetime of charge carriers even in the absence of Pt or ascorbic acid.

As it can be noticed in the above discussion, the photocatalyst for hydrogen production under UV-visible light may be a donor or acceptor or a heterojunction composed of two materials which must be designed to make it both the donor and the acceptor. Nevertheless, in CQD/semiconductor-based photocatalysts, CQDs serve as both the acceptor and the donor. Under UV light illumination, CQDs serve as the acceptor and under visible light illumination, CQDs serve as the donor, making the photocatalyst efficient and best suited for hydrogen production compared to other photocatalysts.

4. Challenges in photocatalyst design

The challenges involved in designing CQD/semiconductor-based photocatalysts are summarized in Fig. 13.

The CQD/semiconductor-based photocatalysts have several challenges in producing hydrogen by photocatalytic water

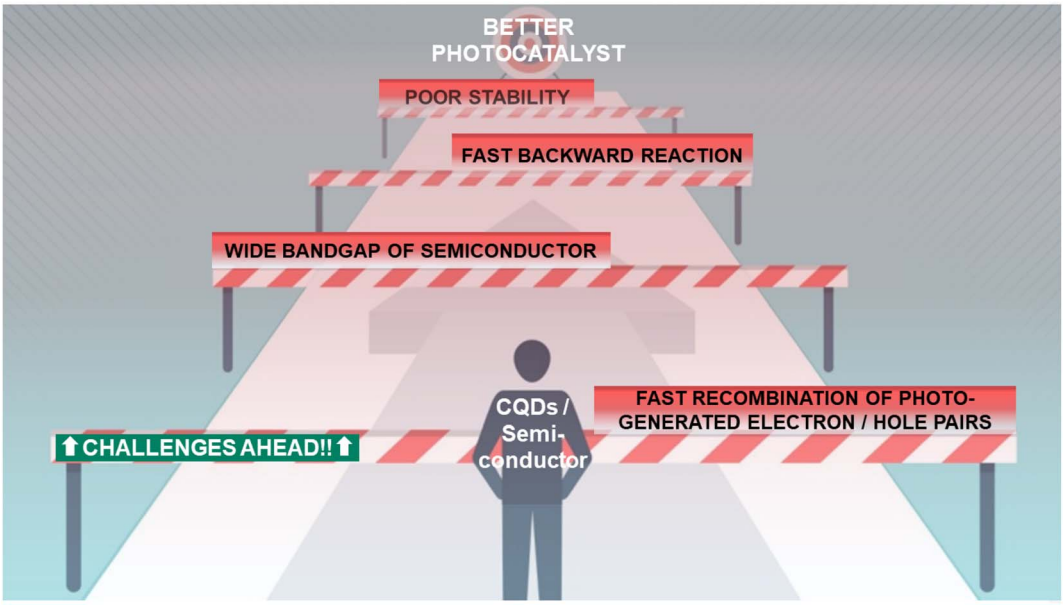

Fig. 13 Challenges of CQD/semiconductor-based photocatalysts.

splitting such as the recovery of photocatalysts, safety issues with cogeneration of hydrogen and oxygen, and less conversion efficiency of solar to hydrogen (STH).[87,88] The current overall STH conversion efficiency is ~5% and the commercial viability of this technology requires a STH conversion efficiency of ~10%.[89] Some of the crucial challenges are listed below.

(1) Several photocatalysts are active only under UV light due to its large bandgap. To be of practical use, the light absorption and hydrogen conversion rate of the catalysts should be within the visible light spectrum.

(2) Visible light accounts for ~43% of the solar radiation on the surface of the earth compared to ~3–5% of UV light. Consequently, the optimal photocatalyst should operate in the visible-light spectrum with a bandgap less than 3 eV.

(3) High photogenerated charge carrier recombination rate and poor charge separation and transport.

(4) Poor stability of the photocatalysts under the reaction conditions, photo-corrosion, oxidation, agglomeration, or deactivation after the photocatalytic reaction.

(5) The back reaction in the photo-reactor to form H_2O from the evolved hydrogen and oxygen gases.

5. Summary and perspectives

The photocatalytic hydrogen production using CQD/semiconductor-based photocatalysts is an alternative to the depletion of fossil fuels. The semiconductors suffer from wide band, fast recombination of photogenerated electron–hole pairs, and photo corrosion, and are unable to be active in the visible region. The coupling of semiconductors with CQDs will enhance the efficiency of photocatalytic hydrogen production. CQDs serve as the electron reservoir under ultraviolet light illumination and the photosensitiser for semiconductors under visible light illumination. The coupling of CQDs with semiconductors decreases the band gap, suppresses the recombination of photogenerated electron–hole pairs, increases the lifetime of photogenerated charge carriers, and increases the cycling stability, thereby making the CQDs/semiconductor promising for practical applications. Further, the doping and co-doping of CQDs enhance the photocatalytic hydrogen production of the CQDs/semiconductor as dopants or co-dopants provide some additional energy levels above the VB of CQDs, leading to a shift of the Fermi level towards the CB, thereby transferring photogenerated electrons faster. Further, the hydrogen production efficiency of the CQDs/semiconductor can be improved by co-doping three heteroatoms to CQDs, introducing co-catalysts. Despite all these, there are still numerous opportunities to explore the immense applications of CQDs for energy conversion and energy storage.

Data availability

No primary research results, software or code have been included and no new data were generated or analyzed as part of this review.

Conflicts of interest

There are no conflicts to declare.

References

1 X. Xu, R. Ray, Y. Gu, H. J. Ploehn, L. Gearheart, K. Raker and W. A. Scrivens, Electrophoretic analysis and purification of fluorescent single-walled carbon nanotube fragments, *J. Am. Chem. Soc.*, 2004, **126**, 12736–12737.
2 Y. P. Sun, B. Zhou, Y. Lin, W. Wang, K. A. S. Fernando, P. Pathak, M. J. Meziani, B. A. Harruff, X. Wang, H. Wang,

P. G. Luo, H. Yang, M. E. Kose, B. Chen, L. M. Veca and S. Y. Xie, Quantum-sized carbon Dots for bright and colorful photoluminescence, *J. Am. Chem. Soc.*, 2006, **128**, 7756–7757.

3 S. Zhu, Q. Meng, L. Wang, J. Zhang, Y. Song, H. Jin, K. Zhang, H. Sun, H. Wang and B. Yang, Highly photoluminescent carbon dots for multicolor patterning, sensors, and bioimaging, *Angew. Chem., Int. Ed.*, 2013, **52**, 3953–3957.

4 J. Liu, R. Li and B. Yang, Carbon dots: A new type of carbon-based nanomaterial with wide applications, *ACS Cent. Sci.*, 2020, **6**, 2179–2195.

5 A. Ghaffarkhah, E. Hosseini, M. Kamkar, A. A. Sehat, S. Dordanihaghighi, A. Allahbakhsh, C. van der Kuur and M. Arjmand, Synthesis, applications, and prospects of graphene quantum dots: A comprehensive review, *Small*, 2022, **18**, 2102683.

6 S. Tao, T. Feng, C. Zheng, S. Zhu and B. Yang, Carbonized polymer dots: A brand new perspective to recognize luminescent carbon-based nanomaterials, *J. Phys. Chem. Lett.*, 2019, **10**, 5182–5188.

7 R. Wang, K. Q. Lu, Z. R. Tang and Y. J. Xu, Recent progress in carbon quantum dots: synthesis, properties and applications in photocatalysis, *J. Mater. Chem. A*, 2017, **5**, 3717–3734.

8 S. Y. Lim, W. Shen and Z. Gao, Carbon quantum dots and their applications, *Chem. Soc. Rev.*, 2015, **44**, 362–381.

9 A. Vibhute, T. Patil, R. Gambhir and A. P. Tiwari, Photocatalytic hydrogen production using metal doped TiO2: A review of recent advances, *Appl. Surf. Sci. Adv.*, 2022, **11**, 100311.

10 J. Xiao, R. Momen and C. Liu, Application of carbon quantum dots in supercapacitors: A mini review, *Electron. Commun.*, 2021, **132**, 107143.

11 M. J. Molaei, Principles, mechanisms, and application of carbon quantum dots in sensors: a review, *Anal. Methods*, 2020, **12**, 1266–1287.

12 A. Kim, J. K. Dash, P. Kumar and R. Patel, Carbon-based quantum dots for photovoltaic devices: A review, *ACS Appl. Electron. Mater.*, 2022, **4**, 27–58.

13 Y. Shi, Z. Wang, T. Meng, T. Yuan, R. Ni, Y. Li, X. Li, Y. Zhang, Z. Tan, S. Lei and L. Fan, Red phosphorescent carbon quantum dot organic framework-based electroluminescent light-emitting diodes exceeding 5% external quantum efficiency, *J. Am. Chem. Soc.*, 2021, **143**, 18941–18951.

14 B. Zhao and Z. Tan, Fluorescent carbon dots: Fantastic electroluminescent materials for light-emitting diodes, *Adv. Sci.*, 2021, **8**, 2001977.

15 V. D. Sharma, V. Vishal, G. Chandan, A. Bhatia, S. Chakrabarti and M. K. Bera, Green, sustainable, and economical synthesis of fluorescent nitrogen doped carbon quantum dots for applications in optical displays and light-emitting diodes, *Mater. Today Sustain.*, 2022, **19**, 100184.

16 H. Guo, Z. Liu, X. Shen and L. Wang, One-pot synthesis of orange emissive carbon quantum dots for all-type high color rendering index white light-emitting diodes, *ACS Sustainable Chem. Eng.*, 2022, **10**, 8289–8296.

17 B. C. M. Martindale, G. A. M. Hutton, C. A. Caputo and E. Reisner, Solar hydrogen production using carbon quantum dots and a molecular nickel catalyst, *J. Am. Chem. Soc.*, 2015, **137**, 6018–6025.

18 A. S. Patra, G. Gogoi and M. Qureshi, Ordered-Disordered $BaZrO_3-\delta$ hollow nanosphere/carbon dot hybrid nanocomposite: A new visible-light-driven efficient composite photocatalyst for hydrogen production and dye degradation, *ACS Omega*, 2018, **3**, 10980–10991.

19 H. Zhao, X. Yu, C. F. Li, W. Yu, A. Wang, Z. Y. Hu, S. Larter, Y. Li, M. G. Kibria and J. Hu, Carbon quantum dots modified TiO_2 composites for hydrogen production and selective glucose photo reforming, *J. Energy Chem.*, 2022, **64**, 201–208.

20 K. G. Nguyen, I. A. Baragau, R. Gromicova, A. Nicolaev, S. A. J. Thomson, A. Rennie, N. P. Power, M. T. Sajjad and S. Kellici, Investigating the effect of N-doping on carbon quantum dots structure, optical properties and metal ion screening, *Sci. Rep.*, 2022, **12**, 13806.

21 G. Kalaiyarasan, J. Joseph and P. Kumar, Phosphorus-doped carbon quantum dots as fluorometric probes for iron detection, *ACS Omega*, 2020, **5**, 22278–22288.

22 Q. Xu, P. Pu, J. Zhao, C. Dong, C. Gao, Y. Chen, J. Chen, Y. Liu and H. Zhou, Preparation of highly photoluminescent sulfur-doped carbon dots for Fe(iii) detection, *J. Mater. Chem. A*, 2015, **3**, 542–546.

23 A. R. Anju, K. Rawat, T. Prasad and H. B. Bohidar, Boron-doped carbon quantum dots: a 'turn-off' fluorescent probe for dopamine detection, *Nanotechnology*, 2020, **32**, 025501.

24 F. Li, T. Li, C. Sun, J. Xia, Y. Jiao and H. Xu, Selenium-doped carbon quantum dots for free-radical scavenging, *Angew. Chem., Int. Ed.*, 2017, **56**, 9910–9914.

25 H. J. Yashwanth, S. R. Rondiya, N. Y. Dzade, R. L. Z. Hoye, R. J. Choudhary, D. M. Phase, S. D. Dhole and K. Hareesh, Improved photocatalytic activity of TiO_2 nanoparticles through nitrogen and phosphorus co-doped carbon quantum dots: an experimental and theoretical study, *Phys. Chem. Chem. Phys.*, 2022, **24**, 15271–15279.

26 H. J. Yashwanth, S. R. Rondiya, H. I. Eya, N. Y. Dzade, D. M. Phase, S. D. Dhole and K. Hareesh, Synergy between nitrogen, phosphorus co-doped carbon quantum dots and ZnO nanorods for enhanced hydrogen production, *J. Alloys Compd.*, 2023, **937**, 168397.

27 G. Magdy, S. Ebrahim, F. Belal, R. A. El-Domany and A. M. Abdel-Magied, Sulfur and nitrogen co-doped carbon quantum dots as fluorescent probes for the determination of some pharmaceutically important nitro compounds, *Sci. Rep.*, 2023, **13**, 5502.

28 L. Zhu, D. Shen and K. H. Luo, Triple-emission nitrogen and boron co-doped carbon quantum dots from lignin: Highly fluorescent sensing platform for detection of hexavalent chromium ions, *J. Colloid Interface Sci.*, 2022, **617**, 557–567.

29 A. Gupta, B. Likozar, R. Jana, W. C. Chanu and M. K. Singh, A review of hydrogen production processes by photocatalytic water splitting – From atomistic catalysis design to optimal reactor engineering, *Int. J. Hydrogen Energy*, 2022, **47**, 33282–33307.

30 J. H. Chang, M. Kumar and S. Y. Shen, Fundamentals of photoelectrochemical water splitting, *Nanostructured materials for photoelectrochemical water splitting*, ed. J. H. Chang, M. Kumar and A. K. Nayak, IOP publisher, 2021, ch. 1, pp. 1–20.

31 X. Chen, S. Shen, L. Guo and S. S. Mao, Semiconductor-based photocatalytic hydrogen generation, *Chem. Rev.*, 2010, **110**, 6503–6570.

32 K. Yamaguti and S. Sato, Photolysis of water over metallized powdered titanium dioxide, *J. Chem. Soc., Faraday Trans. 1*, 1985, **81**, 1237–1246.

33 E. Borgarello, J. Kiwi, M. Gratzel, E. Pelizzetti and M. Visca, Visible light induced water cleavage in colloidal solutions of chromium-doped titanium dioxide particles, *J. Am. Chem. Soc.*, 1982, **104**, 2996–3002.

34 H. Kato, H. Kobayashi and A. Kudo, Role of Ag^+ in the band structures and photocatalytic properties of $AgMO_3$ (M: Ta and Nb) with the perovskite structure, *J. Phys. Chem. B*, 2002, **106**, 12441–12447.

35 H. G. Kim, O. S. Becker, J. S. Jang, S. M. Ji, P. H. Borse and J. S. Lee, A generic method of visible light sensitization for perovskite-related layered oxides: Substitution effect of lead, *J. Solid State Chem.*, 2006, **179**, 1214–1218.

36 D. Li, J. Zheng and Z. Zou, Band structure and photocatalytic properties of perovskite-type compound Ca_2NiWO_6 for water splitting, *J. Phys. Chem. Solids*, 2006, **67**, 801–806.

37 J. Yin, Z. Zou and J. Ye, Photophysical and photocatalytic properties of new photocatalysts $MCrO_4$ (M=Sr, Ba), *Chem. Phys. Lett.*, 2003, **378**, 24–28.

38 M. Matsumura, Y. Saho and H. Tsubomura, Photocatalytic hydrogen production from solutions of sulfite using platinized cadmium sulfide powder, *J. Phys. Chem.*, 1983, **87**, 3807–3808.

39 J. F. Reber and K. Meier, Photochemical production of hydrogen with zinc sulfide suspensions, *J. Phys. Chem.*, 1984, **88**, 5903.

40 T. Shimidzu, T. Iyoda and Y. Koide, An advanced visible-light-induced water reduction with dye-sensitized semiconductor powder catalyst, *J. Am. Chem. Soc.*, 1985, **107**, 35–41.

41 X. Li, N. Sun, Y. Bai, Y. Yan, T. Ouyang, X. Wang, X. Jiang, Z. Wang, X. Cai, J. Cai and H. Tan, High photocatalytic hydrogen production of $Ag@TiO_2$ with different sizes by simple chemical synthesis, *Langmuir*, 2023, **39**, 3350–3357.

42 X. Wang, G. Liu, Z. Chen, F. Li, L. Wang, G. Lu and H. Cheng, Enhanced photocatalytic hydrogen evolution by prolonging the lifetime of carriers in ZnO/CdS heterostructures, *Chem. Commun.*, 2009, **23**, 3452–3454.

43 K. Hareesh, S. D. Dhole, D. M. Phase and J. F. Williams, One-step bacterial assisted synthesis of CdS/rGO nanocomposite as Hydrogen production catalyst, *Mater. Res. Bull.*, 2019, **110**, 82–89.

44 Y. Zhu, Q. Ling, Y. Liu, H. Wang and Y. Zhu, Photocatalytic H_2 evolution on MoS_2-TiO_2 catalysts synthesized via mechanochemistry, *Phys. Chem. Chem. Phys.*, 2015, **17**, 933–940.

45 S. Liang, G. Sui, D. Guo, Z. Luo, R. Xu, H. Yao, J. Li and C. Wang, *J. Colloid Interface Sci.*, 2023, **635**, 83–93.

46 K. Liang, M. Yin, D. Ma, Y. Fan and Z. Li, Facile preparation and photocatalytic hydrogen production of WS_2 and its composites, *Int. J. Hydrogen Energy*, 2022, **47**, 38622–38634.

47 P. Chen, L. Wang, P. Wang, A. Kostka, M. Wark, M. Muhler and R. Beranek, CNT-TiO_2 composites for improved co-catalyst dispersion and stabilized photocatalytic hydrogen production, *Catalysts*, 2015, **5**, 270–285.

48 J. S. Jang, H. G. Kim, U. A. Joshi, J. W. Jang and J. S. Lee, Fabrication of CdS nanowires decorated with TiO_2 nanoparticles for photocatalytic hydrogen production under visible light irradiation, *Int. J. Hydrogen Energy*, 2008, **33**, 5975–5980.

49 Z. Wang, T. Hu, H. He, Y. Fu, X. Zhang, J. Sun, L. Xing, B. Liu, Y. Zhang and X. Xue, Enhanced H_2 production of TiO_2/ZnO Nanowires co-using solar and mechanical energy through piezo-photocatalytic effect, *ACS Sustainable Chem. Eng.*, 2018, **6**, 10162–10172.

50 H. Yu, Y. Zhao, C. Zhou, L. Shang, Y. Peng, Y. Cao, L. Z. Wu, C. H. Tung and T. Zhang, Carbon quantum dots/TiO_2 composites for efficient photocatalytic hydrogen evolution, *J. Mater. Chem. A*, 2014, **2**, 3344–3351.

51 Y. Sui, L. Wu, S. Zhong and Q. Liu, Carbon quantum dots/TiO_2 nanosheets with dominant (001) facets for enhanced photocatalytic hydrogen evolution, *Appl. Surf. Sci.*, 2019, **480**, 810–816.

52 I. Sargin, G. Yanalak, G. Arslan and I. H. Patir, Green synthesized carbon quantum dots as TiO_2 sensitizers for photocatalytic hydrogen evolution, *Int. J. Hydrogen Energy*, 2019, **44**, 21781–21789.

53 J. Zhang, Q. Liu, J. Wang, H. He, F. Shi, B. Xing, J. Jia, G. Huang and C. Zhang, Facile preparation of carbon quantum dots/TiO_2 composites at room temperature with improved visible-light photocatalytic activity, *J. Alloys Compd.*, 2021, **869**, 159389.

54 Y. Zhou, S. Yang, D. Fan, J. Reilly, H. Zhang, W. Yao and J. Huang, Carbon quantum dot/TiO_2 nanohybrids: Efficient photocatalysts for hydrogen generation via intimate contact and efficient charge separation, *ACS Appl. Nano Mater.*, 2019, **2**, 1027–1032.

55 Y. Tang, R. Hao, Y. Fu, Y. Jiang, X. Zhang, Q. Pan and B. Jiang, Carbon quantum dot/mixed crystal TiO_2 composites via a hydrogenation process: an efficient photocatalyst for the hydrogen evolution reaction, *RSC Adv.*, 2016, **6**, 96803–96808.

56 X. Huang, L. Sun, X. Liu, M. Ge, B. Zhao, Y. Bai, Y. Wang, S. Han, Y. Li, Y. Han and C. Zhang, Increase and enrichment of active electrons by carbon dots induced to improve TiO_2 photocatalytic hydrogen production activity, *Appl. Surf. Sci.*, 2023, **630**, 157494.

57 B. Wang, Z. Deng, X. Fu and Z. Li, MoS_2/CQDs obtained by photoreduction for assembly of a ternary MoS_2/CQDs/$ZnIn_2S_4$ nanocomposite for efficient photocatalytic hydrogen evolution under visible light, *J. Mater. Chem. A*, 2018, **6**, 19735–19742.

58 Z. Qu, J. Wang, J. Tang, X. Shu, X. Liu, Z. Zhang and J. Wang, Carbon quantum dots/$KNbO_3$ hybrid composites with enhanced visible-light driven photocatalytic activity toward dye waste-water degradation and hydrogen production, *Mol. Catal.*, 2018, **445**, 1–11.

59 Y. Wang, J. Chen, L. Liu, X. Xi, Y. Li, Z. Geng, G. Jiang and Z. Zhao, Novel metal doped carbon quantum dots/CdS composites for efficient photocatalytic hydrogen evolution, *Nanoscale*, 2019, **11**, 1618–1625.

60 F. Li, Y. Liu, B. Mao, L. Li, H. Huang, D. Zhang, W. Dong, Z. Kang and W. Shi, Carbon-dots-mediated highly efficient hole transfer in I-III-VI quantum dots for photocatalytic hydrogen production, *Appl. Catal., B*, 2021, **292**, 120154.

61 Y. Vyas, P. Chundawat, D. Dharmendra, P. B. Punjabi and C. Ameta, Review on hydrogen production photocatalytically using carbon quantum dots: Future fuel, *Int. J. Hydrogen Energy*, 2021, **46**, 37208–37241.

62 S. Xu, M. Li, Y. Wang and Z. Jin, Enhanced photocatalytic hydrogen evolution over coal-based carbon quantum dots modified $CoMoO_4$/g-C_3N_4, *Int. J. Hydrogen Energy*, 2024, **51**, 16–30.

63 S. Xu, Y. Wang, Y. Wu and M. Li, Nitrogen and sulfur co-doped coal-based carbon quantum dots enhance the photocatalytic hydrogen evolution of Co-Fe-P derived from MOF, *Surf. Inter.*, 2024, **44**, 103576.

64 J. Jia, Y. Sun, Y. Zhang, Q. Liu, J. Cao, G. Huang, B. Xing, C. Zhang, L. Zhang and Y. Cao, Facile and efficient fabrication of bandgap tunable carbon quantum dots derived from anthracite and their photoluminescence properties, *Front. Chem.*, 2020, **8**, 123.

65 A. Mehta, D. Pooja, A. Thakur and S. Basu, Enhanced photocatalytic water splitting by gold carbon dot core shell nanocatalyst under visible/sunlight, *New J. Chem.*, 2017, **41**, 4573–4581.

66 A. S. Patra, G. Gogoi and M. Qureshi, Ordered–Disordered $BaZrO_{3-\delta}$ hollow nanosphere/carbon dot hybrid nanocomposite: A new visible-light-driven efficient composite photocatalyst for hydrogen production and dye degradation, *ACS Omega*, 2018, **3**, 10980–10991.

67 D. Gogoi, R. Koyani, A. K. Golder and N. R. Peela, Enhanced photocatalytic hydrogen evolution using green carbon quantum dots modified 1-D CdS nanowires under visible light irradiation, *Sol. Energy*, 2020, **208**, 966–977.

68 S. Manchala, A. Gandamalla, N. R. Vempuluru, S. M. Venkatakrishnan and V. Shanker, High potential and robust ternary $LaFeO_3$/CdS/carbon quantum dots nanocomposite for photocatalytic H_2 evolution under sunlight illumination, *J. Colloid Interface Sci.*, 2021, **583**, 255–266.

69 J. Hou, H. Cheng, C. Yang, O. Takeda and H. Zhu, Hierarchical carbon quantum dots/hydrogenated-γ-TaON heterojunctions for broad spectrum photocatalytic performance, *Nano Energy*, 2015, **18**, 143–153.

70 K. Wang, X. Wang, H. Pan, Y. Liu, S. Xu and S. Cao, In situ fabrication of CDs/g-C_3N_4 hybrids with enhanced interface connection via calcination of the precursors for photocatalytic H_2 evolution, *Int. J. Hydrogen Energy*, 2018, **43**, 91–99.

71 L. Zhang, J. Zhang, Y. Xia, M. Xun, H. Chen, X. Liu and X. Yin, Metal-free carbon quantum dots implant graphitic carbon nitride: Enhanced photocatalytic dye wastewater purification with simultaneous hydrogen production, *Int. J. Mol. Sci.*, 2020, **21**, 1052.

72 K. Li, F. Y. Su and W. D. Zhang, Modification of g-C_3N_4 nanosheets by carbon quantum dots for highly efficient photocatalytic generation of hydrogen, *Appl. Surf. Sci.*, 2016, **375**, 110–117.

73 G. Zhang, Q. Ji, Z. Wu, G. Wang, H. Liu, J. Qu and J. Li, Facile "Spot-Heating" synthesis of carbon dots/carbon nitride for solar hydrogen evolution synchronously with contaminant decomposition, *Adv. Funct. Mater.*, 2018, **28**, 1706462.

74 H. Liu, J. Liang, S. Fu, L. Li, J. Cui, P. Gao, F. Zhao and J. Zhou, N doped carbon quantum dots modified defect-rich g-C_3N_4 for enhanced photocatalytic combined pollution degradation and hydrogen evolution, *Colloids Surf., A*, 2020, **591**, 124552.

75 J. Pan, M. You, C. Chi, Z. Dong, B. Wang, M. Zhu, W. Zhao, C. Song, Y. Zheng and C. Li, The two dimension carbon quantum dots modified porous g-C_3N_4/TiO_2 nano-heterojunctions for visible light hydrogen production enhancement, *Int. J. Hydrogen Energy*, 2018, **43**, 6586–6593.

76 R. Shi, Z. Li, H. Yu, L. Shang, C. Zhou, G. I. N. Waterhouse, L. Z. Wu and T. Zhang, Effect of nitrogen doping level on the performance of N-doped carbon quantum dot/TiO_2 composites for photocatalytic hydrogen evolution, *ChemSusChem*, 2017, **10**, 4650–4656.

77 S. Xu, M. Li, Y. Wang, C. Gao, R. Xu and Z. Jin, Enhanced photocatalytic hydrogen production from Co-MOF/CN by nitrogen and sulfur co-doped coal-based carbon quantum dots, *J. Rare Earths*, 2024, **42**(5), 838–850.

78 H. Zhu, L. Gou, C. Li, X. Fu, Y. Weng, L. Chen, B. Fang, L. Shuai and G. Liao, Dual interfacial electric fields in black phosphorus/MXene/MBene enhance broad-spectrum carrier migration efficiency of photocatalytic devices, *Device*, 2024, **2**, 100283.

79 Y. Liu, W. Yin, Q. Lin, Z. Li, W. Zhong and B. Fang, Nitrogen vacancies-engineered graphitic carbon nitride nanosheets for boosting photocatalytic H_2 production, *Appl. Surf. Sci.*, 2023, **640**, 158386.

80 W. H. Lee, C. W. Lee, G. D. Cha, B. H. Lee, J. H. Jeong, H. Park, J. Heo, M. S. Bootharaju, S. H. Sunwoo, J. H. Kim, K. H. Ahn, D. H. Kim and T. Hyeon, Floatable photocatalytic hydrogel nanocomposites for large-scale solar hydrogen production, *Nat. Nanotechnol.*, 2023, **18**, 754–762.

81 C. Li, R. Jia, B. Fang and G. Liao, A floatable hydrogel-based photocatalytic system for large-scale solar hydrogen production, *Appl. Mater. Today*, 2023, **35**, 101930.

82 T. Suguro, F. Kishimoto, N. Kariya, T. Fukui, M. Nakabayashi, N. Shibata, T. Takata, K. Domen and K. Takanabe, A hygroscopic nano-membrane coating achieves efficient vapor-fed photocatalytic water splitting, *Nat. Commun.*, 2022, **13**, 5698.

83 G. Liao, B. Fang and C. Li, A high-pressure-tolerant vapor-fed photocatalytic system for efficient water splitting, *Chem Catal.*, 2023, **3**, 100671.
84 G. Liao, C. Li and B. Fang, An innovative synthesis strategy for high-efficiency and defects switchable-hydrogenated TiO_2 photocatalysts, *Matter*, 2022, **5**, 377–389.
85 S. Yu, Q. Wang, J. Wang, C. Fang, Y. Li, J. Ge and B. Fang, Computational modeling guided design of metal–organic frameworks for photocatalysis – a mini review, *Catal. Sci. Technol.*, 2023, **13**, 6583–6603.
86 G. Liao, C. Li and B. Fang, Donor-acceptor organic semiconductor heterojunction nanoparticles for efficient photocatalytic H_2 evolution, *Matter*, 2022, **5**, 1627–1644.
87 V. Kumaravel, S. Mathew, J. Bartlett and S. C. Pillai, Photocatalytic hydrogen production using metal doped TiO_2 A review of recent advances, *Appl. Catal., B*, 2018, **244**, 1021–1064.
88 P. D. Nguyen, T. M. Duong and P. D. Tran, Current progress and challenges in engineering viable artificial leaf for solar water splitting, *J. Sci.: Adv. Mater. Devices*, 2017, **2**, 399–417.
89 S. K. Lakhera, A. Rajan, T. P. Rugma and N. Bernaurdshaw, A review on particulate photocatalytic hydrogen production system: Progress made in achieving high energy conversion efficiency and key challenges ahead, *Renewable Sustainable Energy Rev.*, 2021, **152**, 111694.